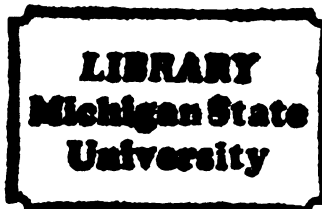




102
713
THS



This is to certify that the

thesis entitled

Heavy Ion Dynamics in a TDHF-Based Classical
Description

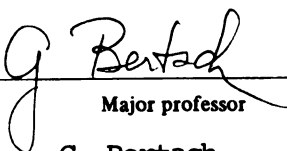
presented by

Aldo Bonasera

has been accepted towards fulfillment
of the requirements for

M.S. degree in Physics

Date 2/20/85


Major professor
G. Bertach



RETURNING MATERIALS:

Place in book drop to
remove this checkout from
your record. FINES will
be charged if book is
returned after the date
stamped below.

--	--	--

HEAVY ION DYNAMICS IN A TDHF-BASED CLASSICAL DESCRIPTION

By

Aldo Bonasera

A THESIS

Submitted to
Michigan State University
in partial fulfillment of the requirements
for the degree of

MASTER OF SCIENCE

Department of Physics and Astronomy

1985

532-3924

ABSTRACT

HEAVY ION DYNAMICS IN A TDHF-BASED CLASSICAL DESCRIPTION

By

Aldo Bonasera

We reduce the TDHF equations of two colliding nuclei to a classical form. These equations mimic the actual behavior of finite nucleus TDHF quite well. The calculated fusion cross sections are in good agreement with experimental data for light and heavy nuclei. The fusion threshold for heavy nuclei is well above the interaction barrier, in agreement with the "extra push" systematics. An interesting feature of our approach is the clear distinction of two different states after neck formation. The first stage is superfluid, while in the second stage there is a strong damping (superviscosity). The occurrence of superviscosity in the rebounding phase is not sufficient to give cold fusion in heavy systems, but does result in a long interaction time. This could be a signature of fast fission. At higher energies the approaching phase is entirely superfluid and explains the window in the fusion cross section seen in TDHF for light nuclei.

TABLE OF CONTENTS

List of Figures

Chapter I	1
1.1 Phenomena in heavy ion collisions	1
1.2 Deep inelastic reactions	2
1.3 Fusion cross sections	3
Chapter II	6
Chapter III	11
3.1 Extension of the model	11
3.2 Fusion cross section	17
3.3 Comparison with Extra Push Model	23
Chapter IV	43
4.1 Deep Inelastic Reactions	43
4.2 Comparison with Experimental Data	44
Appendix	51
References	58

LIST OF FIGURES

Figure		Page
3.1a,b	Experimental isoscalar quadrupole and monopole widths versus mass number compared with Eq. (2), full line. Experimental data are from Ref. 11.	13
3.2	Time interval T (see text) versus energy in the C.M. system for the system $^{40}\text{Ca} + ^{40}\text{Ca}$. $E_{\text{CM}} = 100$ MeV, T is equal to the time delay $t_D = 38$ fm/c	19
3.3	Fusion cross section versus energy for the system $^{40}\text{Ca} + ^{40}\text{Ca}$. Data points are from Refs. 16 and 17	21
3.4	Same as Figure 3.2 for the system $^{208}\text{Pb} + ^{64}\text{Ni}$. The time delay t_D is explicitly indicated in the figure.	22
3.5a-f	Fusion cross sections versus energy in the C.M. for different systems. Data points are from Ref. 19	24
3.6a,b	Same as Figure 3.5. Data are from Ref. 20.	31
3.7a-d	Same as Figure 3.5. Experimental data are from Refs. 21 through 25	34
3.8a,b	Reaction (full line) and fusion cross sections (dashed line) calculated using the present model, compared to the results of the "extra-push" model (dots and squares, respectively), Refs. 7 and 8	40
4.1	The energy loss spectrum for the system $^{84}\text{Kr} + ^{209}\text{Bi}$ at $E_{\text{LAB}} = 712$ MeV.	45
4.2	Interaction time and energy loss versus impact parameter for the system $^{58}\text{Ni} + ^{197}\text{Au}$	48
4.3	Same as Figure 4.2 for the system $^{56}\text{Fe} + ^{165}\text{Ho}$	49

CHAPTER I

1.1 Phenomena in heavy ion collision

Heavy ion collisions are a powerful tool to study the structure of nuclei. Many phenomena are found in heavy ion collisions, depending on the many variables at the disposal of the experimenter. In the present work we deal with low energy collisions, i.e. $E_{\text{lab}} < 15 \text{ MeV/u}$. In this energy regime several phenomena occur. We can classify the reaction cross sections into three main types: quasi elastic scattering, deep inelastic and fusion reactions [1-3].

Quasi elastic collisions occurs in reaction in which the surfaces of the two ions have just been in grazing contact. Thus there is a small energy loss and a few nucleons are transferred from one nucleus to the other. Classically we expect that this type of reaction is dominant at large impact parameters.

The second major category of reaction, the strongly damped collision, is characterized by a large energy loss, but with the projectile and target still maintaining something of their identity in the final state.

Fusion occurs when the energy of the colliding nuclei is just above the Coulomb barrier and for small enough impact parameteres (neglect sub barrier fusion).

In this work we will present a model that is suitable for describing the last two types of reactions. In the next sections we

discuss in a greater detail the experimental signatures of these processes. The formalism is presented in chapter II and results are compared with experimental data in chapters III and IV

1.2 Deep inelastic reactions

Extensive experimental results regarding dissipative collisions are presently available. The main features are as follows.

First the projectile and the target are mostly heavy nuclei with mass number $A > 40$. The identity of projectile and target is essentially preserved, although a considerable amount of mass ($\Delta A < 20$) can be transferred. This mass transfer occurs during an interaction time, i.e. the time during which the two nuclei are in contact, of the order of 10^{-21} - 10^{-22} sec. This time is much smaller than the time needed for a complete rotation of the composite system, $\tau_{\text{rot}} \sim 10^{-20}$ sec, thus the angular distribution is strongly anisotropic.

A large amount of kinetic energy is dissipated, see for example fig. 4.1. In the case of $^{84}\text{Kr} + ^{209}\text{Bi}$ at $E_{\text{CM}} = 508$ MeV, the Coulomb energy of two touching spheres is $V = 300$ MeV, using $R_1 + R_2 = 14.4$ fm, where R_i are the radii of the two nuclei. The energy loss would be 200 MeV, if the two fragments separate with no kinetic energy and only the Coulomb potential energy. Greater energy losses are also observed. This implies that the composite system is greatly elongated before it splits, or that small fragments carry off a great amount of energy. Also a large amount of angular momentum, up to $50\hbar$, is transferred from the relative motion into intrinsic excitation.

The measured cross-sections are inclusive because not all the reaction products can be observed. Usually only scattering angle, energy and charge of one fragment are detected. Since the excitation energy is

large, the channels cannot be resolved and therefore, only averaged quantities are observed.

Model calculation and experiments seem to show that deep inelastic collisions cover the range from the fusion to quasi elastic reactions. When the charge of the two nuclei is larger than a critical value, deep inelastic scattering takes also place for zero impact parameter at energies close to the Coulomb barrier. Thus the fusion region is hindered by these processes and possibly for very large charges of both target and projectile, the fusion region completely disappears.

The interaction time is a useful concept in discussing the angular distributions, mass asymmetry and energy sharing in the final state of the collisions. For example in the case mentioned above, the interaction time is of the order of the time of rotation of the coalesced system, therefore the angular distribution is almost isotropic and the initial mass asymmetry is equilibrated. This process resembles fission following fusion but with a shorter interaction time, thus the name of fast-fission (FF). The other extreme case is when the interaction time is very short, say less than 10^{-22} sec. Model calculations predict that thermal equilibrium is reached after a time of the order of 10^{-21} sec. [30]. In this case preequilibrium processes occur, such as prompt emission of light particles: neutrons, protons, alphas or even the breakage of the composite system in three fragments. These processes have recently been observed [4,5].

1.3 Fusion cross sections

The reaction cross section is coincident with the fusion cross section for light nuclei and energies just above the Coulomb barrier. For larger energies and high angular momenta, fusion is replaced by

deep inelastic scattering. These features are shown for example in fig. 2.3. For high energies and even zero impact parameter a 'window' in the fusion cross section is predicted by Time Dependent Hartree-Fock theory (TDHF) [6]. But, presently, there is no experimental evidence for such a process.

For heavier nuclei, as we saw before, the situation is different. The nuclear attraction increases like $R_1 R_2 / (R_1 + R_2)$, but the Coulomb repulsion increases faster, like $Z_1 Z_2$. The net result is that for great charges the Coulomb repulsion is very strong and the nuclear attraction is not sufficient to keep the nuclei in a coalesced shape. Thus an extra energy ('extra-push') is needed in order to overcome the Coulomb barrier [7,8]. From the above discussion we expect that a critical value, $(Z_1 Z_2)_{thr}$, exists below which fusion occurs as soon as the two nuclei touch. Of course, due to the imprecise knowledge we have of the nucleus-nucleus potential, such threshold value is model dependent.

The fused nuclei have a lifetime of the order of 10^{-17} - 10^{-19} sec. During this time a statistical equilibrium is reached, thus concepts like temperature and entropy are very useful.

The compound nucleus formed in a heavy-ion collision has an excitation energy E^* dependent on the angular momentum. It cools down mainly by evaporation of neutrons or other light particles until it reaches a certain value of E^* after which photons are emitted in cascade. Since the light particles carry a small fraction of the angular momentum of the compound nucleus, a measurement of the γ -multiplicity gives an estimate of the angular momentum near the yrast line.

For high angular momenta where the fission barrier is below 8 MeV, the compound system is more likely to split in two symmetric fragments. For example for the system $^{208}\text{Pb}+^{32}\text{S}$, it is shown that the entire mass of the projectile is transferred to the composite system which subsequently decays via symmetric fission [9].

CHAPTER II

NEWTONIAN DYNAMICS OF TIME-DEPENDENT MEAN FIELD THEORY

A. BONASERA, G.F. BERTSCH and E.N. EL-SAYED

Cyclotron Laboratory, Michigan State University, East Lansing, MI 48824, USA

Received 6 February 1984

Force equations describing heavy ion collisions are derived from the continuum limit of time-dependent mean field theory. The equations mimic the actual behavior of finite nucleus TDHF quite well, and might serve as a starting point for a more complete theory.

In this note we investigate a single model for low energy heavy ion collisions [1], based on the dynamics of time-dependent mean field theory (TDHF). The theory is reduced to the newtonian mechanics of two nuclear centers interacting via classical forces. In view of the many force models that have been put forth already [2-4], it is natural to ask what the point is of yet another such model. Our objective is to understand the fundamental dynamics of the reactions, and this requires a model that is consistent with our present theoretical framework. At present, the TDHF is the best justified theory at a fundamental level, although it is obviously incomplete in several respects and needs to be extended. Because of the computational difficulties of the theory, extensions are unmanageable unless a simple modelling is found for TDHF itself. Our efforts are directed to that end.

The most important dynamic variable in a simplified description is the separation coordinate between the colliding nuclei, r . We begin with a precise definition of that quantity. Consider a plane between the two nuclei chosen so that the expectation of nucleon number on each side remains fixed. Calling the two sides A and B, the separation coordinate may be defined as the integral over the single-particle density,

$$r = \int_A \rho(r') r' d^3r' - \int_B \rho(r') r' d^3r'. \quad (1)$$

In a like manner the momentum of one of the nuclei may be defined

$$p_A = \int_A d^3r ((\vec{\nabla} - \vec{\nabla}')/2i) \rho^{(1)}(r, r')|_{r=r'}. \quad (2)$$

The dynamic equation is found by taking the time derivative of eq. (2), using the hamiltonian to evaluate the derivative of the wave function. In TDHF the hamiltonian is a single-particle operator and the dynamic equation becomes

$$\frac{dp_A}{dt} = \frac{1}{i} \int_A \sum_i [\phi_i^* ((\vec{\nabla} - \vec{\nabla}')/2i) H \phi_i - (H \phi_i^*) ((\vec{\nabla} - \vec{\nabla}')/2i) \phi_i] d^3r. \quad (3)$$

Here ϕ_i are the single-particle wave functions and H is the TDHF hamiltonian. The terms in eq. (3) involving the kinetic energy operator are simplified in the usual way using integration by parts, leaving a surface integral. We assume that the mean field potential depends only on the single-particle density, permitting an arbitrary functional dependence on that density. The contribution of the short range part of the potential field can then also be expressed as a surface integral on the dividing plane. The resulting equation for the acceleration has the form

$$\begin{aligned} \frac{dp_A}{dt} = & \int_S d^2r [\vec{n} \cdot \Pi + \vec{n} (\rho \partial U / \partial \rho - U)] \\ & + \int_A d^3r \int_B d^3r' \frac{\rho_p(r) \rho_p(r') e^2}{|r - r'|^3} (r - r'). \end{aligned} \quad (4)$$

The first term is a surface integral involving the particle momentum flux tensor

$$\Pi_{\alpha\beta} = \frac{1}{m} \sum_i \phi_i^* ((\vec{\nabla} - \vec{\nabla})/2i)_\alpha ((\vec{\nabla} - \vec{\nabla})/2i)_\beta \phi_i, \quad (5)$$

and a potential field contribution, which is expressed in terms of the potential energy density associated with the short-range part of the interaction [5], U . The dividing plane is denoted by S and the normal to this surface by \vec{n} . The Coulomb force is given by the second integral in the equation. Eq. (4) is expressed in a form particularly convenient for reduction to classical dynamics. We expect on physical grounds that the force between the two nuclei depends only on the state of the system at the surface of contact, except for the long range Coulomb interaction. Eq. (4) has this form, with the first term in the surface integral arising from the exchange of nucleons between two nuclei. The second term is the force arising from the nuclear potential field. At large separations, the potential dominates because the potential field extends farther than the particle densities. At close contact, the two terms tend to cancel, and the residual force depends sensitively on the momentum distribution of the nucleons and the compressibility modulus associated with the hamiltonian.

In principle, the full TDHF wave function is still needed to calculate the right-hand side of eq. (4); our model is a set of simplifying assumptions about how the TDHF behaves. We shall approximate the TDHF density matrix by its value in bulk nuclear matter, together with a surface correction. Parametrizing the contact surface S as a circle of radius r_n , eq. (4) is reduced to

$$\begin{aligned} dp_A/dt = & \pi r_n^2 \vec{n} \cdot [\Pi + 1(\rho \delta U/\delta \rho - U)]_{NM} \\ & + 2\pi \sigma r_n \vec{n} + (Z_1 Z_2 e^2/r^2) \vec{n}. \end{aligned} \quad (6)$$

The bulk contribution is given by the first term on the right, with the subscript NM denoting a nuclear matter approximation. The surface contribution is proportional to σ , which we take to be the empirical surface energy, $\sigma = 0.9 \text{ MeV/fm}^2$. For the calculations below, we treat the Coulomb interaction in the monopole-monopole approximation, which is quite accurate for lighter nuclei.

In mean field theory, the density matrix for two colliding slabs of nuclear matter is described by two

intersecting Fermi surfaces which may become distorted from spherical shape by potential field effects. If the compressibility of nuclear matter is that of a free Fermi gas, which seems to be close to the empirical situation, then the surfaces are just the Fermi spheres of the individual slabs. The particle flux tensor was evaluated to lowest order in the relative velocity of the two Fermi spheres, v_{nm} by Randrup [6] to give a momentum flux across the surface

$$\vec{n}_0 [\Pi + 1(\rho \delta U/\delta \rho - U)]_{NM} \cong \frac{3}{16} \rho v_F m (\vec{n} \vec{n} \cdot v_{nm} + v_{nm}). \quad (7)$$

Here v_F is the Fermi velocity. Randrup further replaced v_{nm} by dr/dt , in effect assuming that all parts of the nucleus have the same motion. This reduces the force to a linear friction. However, the Fermi surface in mean field dynamics depends on the motion of the boundary of the nucleus at an earlier time, resulting in a lag [7] between the center of mass motion and the local Fermi surface at S . The delay time is certainly more than the nucleon transit time, and is less than twice the transit time. Within these limits, we shall leave the delay time as a parameter, writing it as

$$t_D = \alpha t_0, \quad t_0 = 2R/v_F,$$

where $1 < \alpha < 2$. The transverse part of v_{nm} has contributions both from the center of mass motion and from the internal angular momentum of the individual nuclei. Our model for v_{nm} is then

$$v_{nm}(t) = (dr/dt)(t - t_D) + \vec{s}(R_A l_A/l_A - R_B l_B/l_B), \quad (8)$$

where R , l , and I are the radii, angular momentum, and moment of inertia of the nuclei, and \vec{s} is a unit vector in the reaction plane. The angular momentum can be found from the integration of the force equation, so the only need for a finite nucleus TDHF calculation is the determination of the evolution of the neck radius.

The dynamics of the neck region are quite different when the two nuclei approach each other than when they rebound. The TDHF calculations show that the motion of the nuclei in the approach phase is close to that of rigid spheres [8], with the overlap region of the spheres defining the neck size. The neck only exceeds the geometric overlap slightly at the closest approach point. The geometric overlap assumption was used in refs. [2] and [3]. We shall improve the para-

meterization by assuming that the nuclear surfaces are sections of spheres with centers separated by the distance r , joined by a cylinder of such a radius to make a constant volume solid. The neck radius is obtained from the equation,

$$r_N^2(r - 2r_x) = [r_N^2 + \frac{1}{3}(R - r_x)^2](R - r_x), \quad (9)$$

where $r_x = (R^2 - r_N^2)^{1/2}$.

We emphasize that this parameterization is strictly for convenience in finding the r_N of TDHF: we do not imply that the system evolves with a constant volume or that it has a particular shape.

The neck evolution in the rebound phase is quite different. The neck shrinks rather slowly as the nuclei separate; the TDHF calculation of Dhar and Nilsson [8] obtains a neck shrinkage rate of 1/3 of the separation rate. To establish a function for the neck size in the rebounding phase, we assume a shape of two half spheres connected by two conical surfaces. The radius at the junction of the two cones is determined by fixing the volume of the system. The equation for r_N in the rebound phase is

$$r_N = \{[r^2 R^2 - 4r(rR^2 - 4R^3)]^{1/2} - Rr\}/2r.$$

Despite the crudeness of these geometric assumptions, the model fits the neck evolution of the TDHF calculation of Dhar and Nilsson quite well, as may be seen from fig. 1.

The separation into two nuclei at the end of the rebound phase can take place by two different mechanisms. If the neck is too narrow in relation to its length, an instability driven by surface tension will cause the neck to pinch off. However, fast hydrodynamic flow is possible only when the single-particle

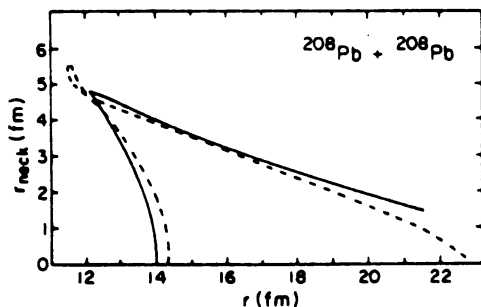


Fig. 1. Relationship between neck radius r_N and separation distance r for $^{208}\text{Pb} + ^{208}\text{Pb}$ collisions at 800 MeV cm energy and zero impact parameter. The solid line is the present model, and the dashed line is from ref. [8].

wave functions are nodeless, requiring a small neck radius. We assume scission to occur when $r_N < 1$ fm. There is another mechanism for neck breakage when the nuclei rebound at high velocity. An instability develops with respect to density fluctuations when the bulk density falls below a critical value. According to ref. [9] this happens in mean field theory when the separation velocity exceeds $0.06c$. We shall assume that the neck snaps when the velocity is exceeded.

So far we have only considered the forces acting after the nuclei touch. Before they touch, the dynamics is well described by potential models, such as the proximity potential [10] or the Bass potential [11]. We shall use the Bass potential to describe the interaction before the nuclei touch. Particle exchange will also be included, using the parameterization of ref. [12].

We shall first examine the detailed motion in the collision $^{40}\text{Ca} + ^{40}\text{Ca}$, to see how well our reduction to force dynamics works. We compare with TDHF

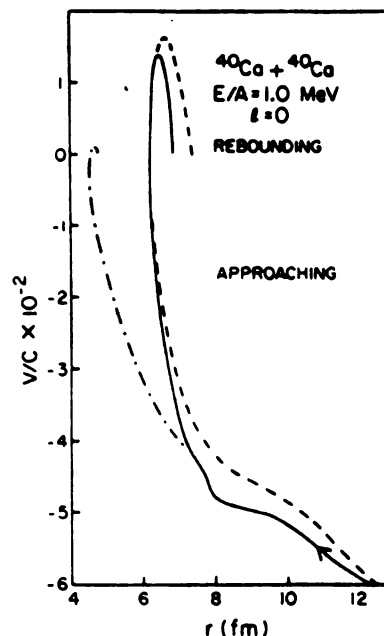


Fig. 2. History of $^{40}\text{Ca} + ^{40}\text{Ca}$ collision at 80 MeV cm energy and zero impact parameter. The solid line shows the velocity as a function of separation distance, and the dashed line is a TDHF calculation by Weiss [13]. The dashed-dotted line shows the result of the force model in which the particle momentum flux is treated as a linear friction.

calculations by Weiss [13] in which r is evaluated as a function of time. In fig. 2 we plot dr/dr as a function of r , for a collision under conditions giving fusion. The figure shows the nuclei slowing down as they approach. At $r = 10$ fm the nuclear attraction is felt and the rate of slowing down diminishes. However, at $r = 6.5$ fm there is a sudden reversal of velocity, as if the nucleus had hit a hard wall and bounced elastically. The strong repulsive force at that point is due to the particle exchange. Our model reproduces that behavior with a memory time constant $\alpha = 1.8$ as shown by the dashed line. Under the assumption of extreme dissipation, $\alpha \sim 0$, and the repulsion does not last long enough to keep the nuclei from approaching to essentially form a spherical compound nucleus. That is shown as the dashed-dotted line in the figure.

We next examine the boundaries of the fusion regime for light nuclei. The TDHF fusion regime for $^{28}\text{Si} + ^{28}\text{Si}$ collisions [14] is shown in fig. 3, compared with our model. The low energy edge is determined by the potential field dynamics. An energy sufficient to surmount the potential barrier will cause the nuclei to touch, and they will remain fused due to the surface tension of the neck. At high impact parameter and energy the nuclei may scission after touching. The boundary line is determined essentially by the balance of centrifugal and surface forces, and may be described by a critical angular momentum. Finally,

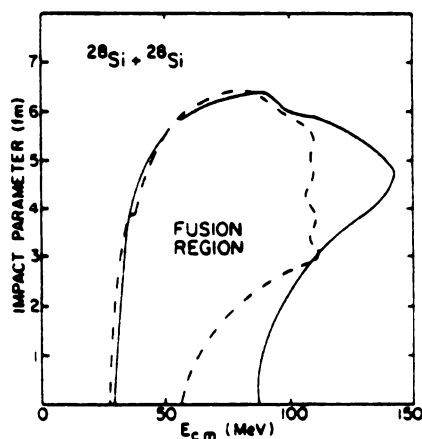


Fig. 3. Behavior of $^{28}\text{Si} + ^{28}\text{Si}$ collisions as a function of impact parameter and initial cm energy. The outer boundary shows the fusion region of the force model. The TDHF fusion prediction [14] is shown enclosed in the dashed line.

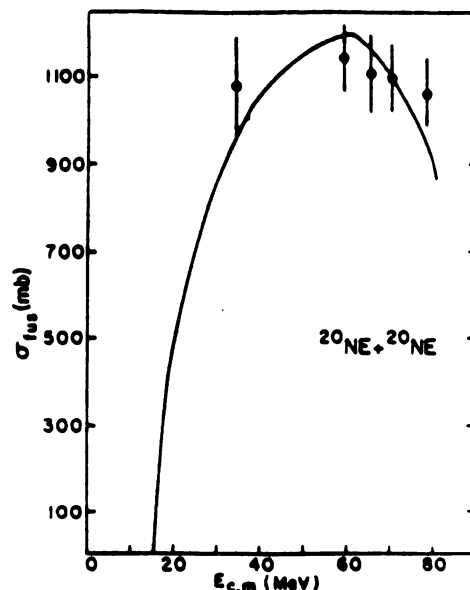


Fig. 4. The experimental fusion cross section for $^{20}\text{Ne} + ^{20}\text{Ne}$ collisions compared with the force model. The decrease in the predicted cross section at the highest energy is due to the opening of the fusion window.

there is a fusion window predicted in TDHF, which arises in our model because of the hard bounce behavior and the possibility of neck breakage at high rebound velocities. Other force models do not have this characteristic feature of TDHF. The comparison of TDHF with our model in fig. 3 shows that all the qualitative features of TDHF can be described with force dynamics.

However, actual nuclear collisions probably do not exhibit fusion windows. In fig. 4 we show the measured fusion cross section [15] for $^{20}\text{Ne} + ^{20}\text{Ne}$ compared with the force model. The experimental cross section is rather constant, even at energies where the fusion window should be evident. Evidently, TDHF is inadequate at the higher energies. Nucleon-nucleon collisions will become important and may affect the force dynamics in several ways. For example, the memory time will be shorter if the system is thermalized by n-n collisions. This will reduce the magnitude of the bounce, leading to more sticking behavior.

We acknowledge the support of the National Science Foundation, and the support of "Fondazione Angelo Della Riccia" for A. Bonasera.

References

- [1] G. Bertsch, MSU preprint (1982).
- [2] D. Gross and H. Kalinowski, Phys. Rep. 45 (1978) 175.
- [3] F. Beck et al., Phys. Lett. 76B (1978) 35.
- [4] D.M. Brink and Fl. Stancu, Phys. Rev. C24 (1981) 144.
- [5] A. Abrikosov and I. Khalatnikov, Rep. Prog. Phys. 22 (1959) 336, eq. (6.3).
- [6] J. Randrup, Ann. Phys. (NY) 112 (1978) 356.
- [7] A. Jain and N. Sarma, Phys. Rev. C24 (1981) 1066.
- [8] A. Dhar and B. Nilsson, Phys. Lett. 77B (1978) 50.
- [9] G. Bertsch and D. Munding, Phys. Rev. C17 (1978) 1646.
- [10] J. Blocki et al., Ann. Phys. (NY) 105 (1977) 427.
- [11] R. Bass, Phys. Rev. Lett. 39 (1977) 265.
- [12] C.M. Ko et al., Phys. Lett. 77B (1978) 174.
- [13] M. Weiss, private communication.
- [14] P. Bonche et al., Phys. Rev. C20 (1979) 641.
- [15] D. Shapiro et al., Phys. Rev. C28 (1983) 1148.

CHAPTER III

3.1 Extension of the model

Encouraged by the success obtained in fitting T.D.H.F., we will now try to extend the model to asymmetric nuclei and compare predictions with experimental data. The mean field theory has been very useful to suggest a good parametrization for the neck radius and also to give an estimate of the time delay. It is also well known that T.D.H.F. gives a correct qualitative description of nuclear dynamics, but due to computational difficulties and to the imprecise knowledge we have of the mean field potential, there is not always a quantitative agreement with data. For example, using the Skyrme II or Skyrme III potential in the reaction $^{86}\text{Kr} + ^{136}\text{La}$, the threshold energy for fusion is shifted by 250 MeV [10]! In the future we will look only for a qualitative explanation of T.D.H.F. and the aim will be to obtain a quantitatively accurate model with few parameters.

Let us discuss first the time delay. One body-dissipation relies on the fact that at low excitation energy the mean free path of nucleons is larger than the nuclear diameters. Dissipation arises only when the nucleons hit the surface of the nucleus. We expect the friction is delayed, to allow the nucleons to cross the entire nucleus and hit the surface opposite to the small window formed between the two colliding nuclei. A similar mechanism acts for giant resonances. In that case we

can imagine a nucleon, excited by the surface oscillation, travelling freely in the nuclear medium and interacting with the mean field, after a time

$$t_d = 2R / \langle v \rangle \quad (1)$$

where R is the radius of the nucleus and $\langle v \rangle = 3/4 v_f$ is the mean velocity in a Fermi gas. This is a characteristic time for the system, and represents the rate of change of the collective energy of the nucleus due to the interaction with different degrees of freedom. According to the uncertainty principle the minimum spread of the energy of the resonance, ΔE , is given by:

$$\Delta E = \hbar / t_d$$

evaluating this formula with standard values for the radius R and the Fermi velocity, we find:

$$\Delta E = 17 A^{-1/3} \text{ MeV} \quad (2)$$

This functional dependence was suggested in ref.[11] as an experimental fit to the empirical data. The wall formula predicts the same A dependence, but the coefficient is about 4 times larger than in equation (2) [12]. This simple estimate works quite well for monopole and quadrupole resonances, as shown in fig.3.1a,b. For higher

Figure 3.1a,b. Experimental isoscalar quadrupole and monopole widths versus mass number compared with Eq. (2), full line. Experimental data are from Ref. 11.

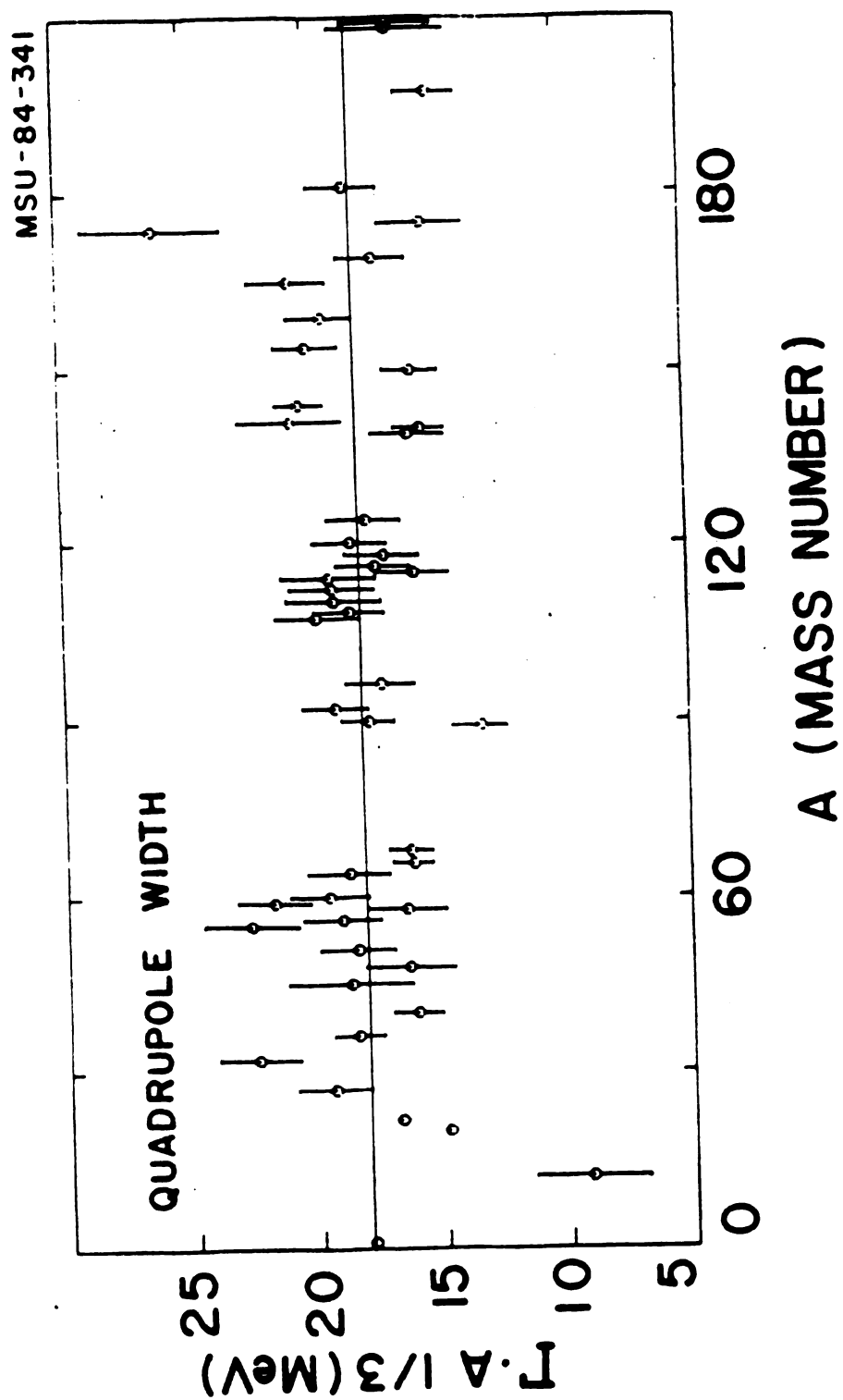


FIGURE 3.1a

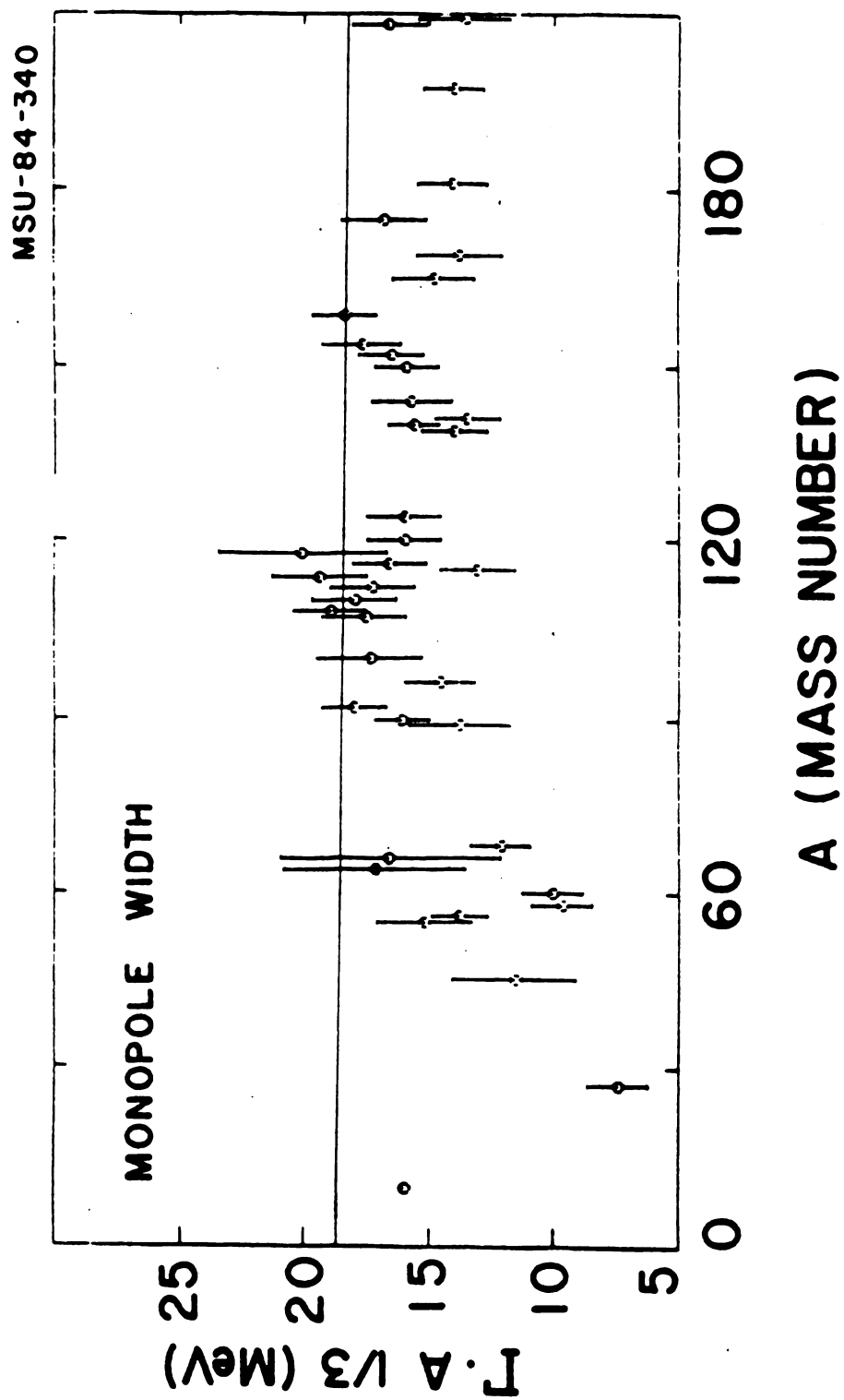


FIGURE 3.1b

multipolarities, in particular the giant octupole resonance, the experimental values are larger than predicted by eq.(2). However, our main purpose is to show the dissipation via a time delay parameter is reasonable and in agreement with dissipation of very collective motion.

In applying the model to asymmetric systems, we treat the nuclei before touching as spheres. The total potential is the same as given before, but we will neglect particle flux through the barrier [31]. The nuclei deform after touching and the simple monopole approximation for the Coulomb field is inadequate. A better parametrization of the Coulomb interaction is given in ref. [13] and we will use this in calculations. The evolution of the neck radius requires in general the introduction of the asymmetry degree of freedom. In order to avoid this difficulty and keep the theory at the simplest level possible, we will rely again on TDHF. Looking carefully to figure (2.1) where the neck radius is plotted versus the relative distance for $^{208}\text{Pb} + ^{208}\text{Pb}$, we notice that the approaching phase resembles a parabola, while the rebounding phase is very close to a straight line. So we will use the equation:

$$r_n = \alpha \cdot \sqrt{R_1 + R_2 - r} \quad (3)$$

where r_n is the neck radius, R_i are the nuclear radii and $\alpha = 3.1 \text{ (fm)}^{1/2}$ is a parameter fitted to TDHF. Note that the neck radius is zero when the nuclei just touch. For the rebounding phase we use:

$$r_n = r_{no} - \beta(r - r_o) \quad (4)$$

with r_{no} and r_o , respectively, the neck radius and the relative distance at the closest approach. $b=.60$ is a parameter fitted to the experimental fusion cross section for $^{64}\text{Ni} + ^{208}\text{Pb}$ at $E_{cm}=395$ MeV. If instead we fit eq (4) to TDHF, we get a larger fusion cross section than experimental data. This is not surprising, in fact, mean field calculations by Stöcker et al. show a general overestimate of data for very heavy systems [14].

The price we have paid to describe nuclear collisions is the introduction of the two parameters in eqs (3) and (4), but still the physical picture beyond the model is simple and clear.

3.2 Fusion cross section

The formation of a compound nucleus requires first of all enough initial kinetic energy to overcome the Coulomb barrier. After touching, the surface tension opposes the Coulomb and centrifugal repulsion. Dissipation plays an important role. It is zero in the first stage after neck formation. In the second stage, the nucleon flux produces a strong pressure which suddenly reduces the relative velocity. This effect has clearly been showed in the reaction $^{40}\text{Ca} + ^{40}\text{Ca}$, (see fig. 2.2). Moreover, this kind of dissipation prevents the two nuclei from reaching a spherical shape. Note that the sudden change between the first stage (superfluidity) and the second stage (superviscidity) can

occur in the approaching phase as well as in the rebounding phase. This is very important and explains the occurrence of neck snap and the possibility of "cold fusion"(see below).

For light nuclei and low angular momentum the nuclear potential at the touching point is much stronger than the repulsive forces; so the nuclei will fuse once they touch. For high angular momentum, the centrifugal barrier will lead the composite system towards scission. The fusion cross section in this region is then mainly determined by the nuclear potential before the nuclei touch; we find the Bass potential to be in good agreement with data. For higher energies, we observe a rupture of the neck at zero impact parameter as well. This is an effect due to the time delay. At low energy, the superviscidity occurs in the approaching phase: the nuclei move then slowly and are trapped. But at higher energies the approaching phase is entirely superfluid: the relative velocity is very high and the occurrence of friction in the rebounding phase is not enough to avoid the overcoming of the critical velocity for neck snap. This effect is demonstrated in fig.3.2, where the time interval $\Delta T = t_c - t_0$ is plotted versus energy. Here t_c and t_0 are the time at the turning and at the touching point respectively. The system is $^{40}\text{Ca} + ^{40}\text{Ca}$ at zero impact parameter. We see that the time interval is larger than t_d up to 100 MeV and in this region we observe fusion. For larger energies the time delay is greater than ΔT , therefore the approaching phase is entirely superfluid and we get neck snap. For the system $^{16}\text{O} + ^{16}\text{O}$, TDHF gives a window in the fusion cross section at energies ranging from 50 to 62 MeV in the laboratory, depending on the Skyrme interaction used. Such a prediction

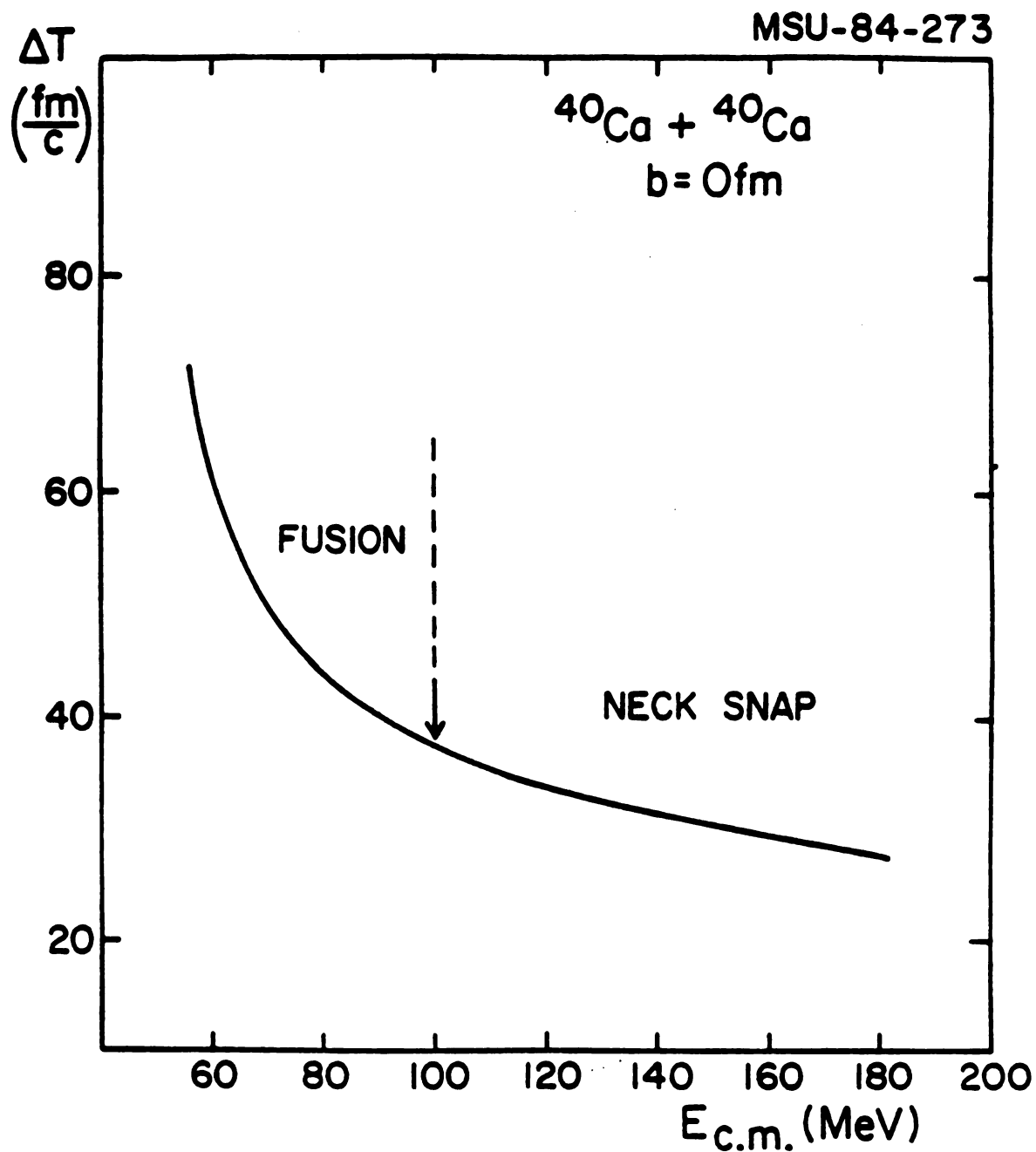


Figure 3.2 Time interval ΔT (see text) versus energy in the C.M. system for the system $^{40}\text{Ca} + ^{40}\text{Ca}$. $E_{\text{CM}} = 100 \text{ MeV}$, T is equal to the time delay $t_D = 38 \text{ fm}/c$.

was tested experimentally at $E_{\text{lab}}=68$ MeV but the results are in disagreement with TDHF [15]. In fig 3.3 we plot the fusion cross section for $^{40}\text{Ca}+^{40}\text{Ca}$. Here two different sets of experimental data are plotted [16,17]. Our model is in better agreement with the data by Tomasi et al. and a repetition of the experiment by Barreto et al. confirms this set [18]. Unfortunately there is only one experimental value at high energy and it is underestimated by our model. However if we add the cross section for neck snap to the fusion cross section we get a value of 1057 mb. This estimate is much larger than the experimental value of 720 mb, thus supporting the existence of the low l-window. The conclusion is that there is still a great uncertainty both in theory and in experiments, suggesting the necessity to repeat these experiments at higher energies.

For very heavy systems the situation is quite different. The Coulomb repulsion is very strong, and the condition that the nuclei touch is not sufficient to get fusion. In this case the role of friction is changed as is clearly seen in fig.3.4 for the system $^{64}\text{Ni}+^{208}\text{Pb}$. At the energy where the nuclei touch, ΔT is just equal to the time delay, therefore the approaching phase is entirely superfluid while the rebounding is superviscid. This situation would, in this case, favor fusion; but the repulsion is too strong for a wide neck to be formed and the nuclei re-separate. For this reason, cold fusion as discussed by Swiatecki [7] cannot occur. The only possibility to get it would be for nuclei having a $(Z^2/A)_{\text{eff}}$ close to the threshold value.

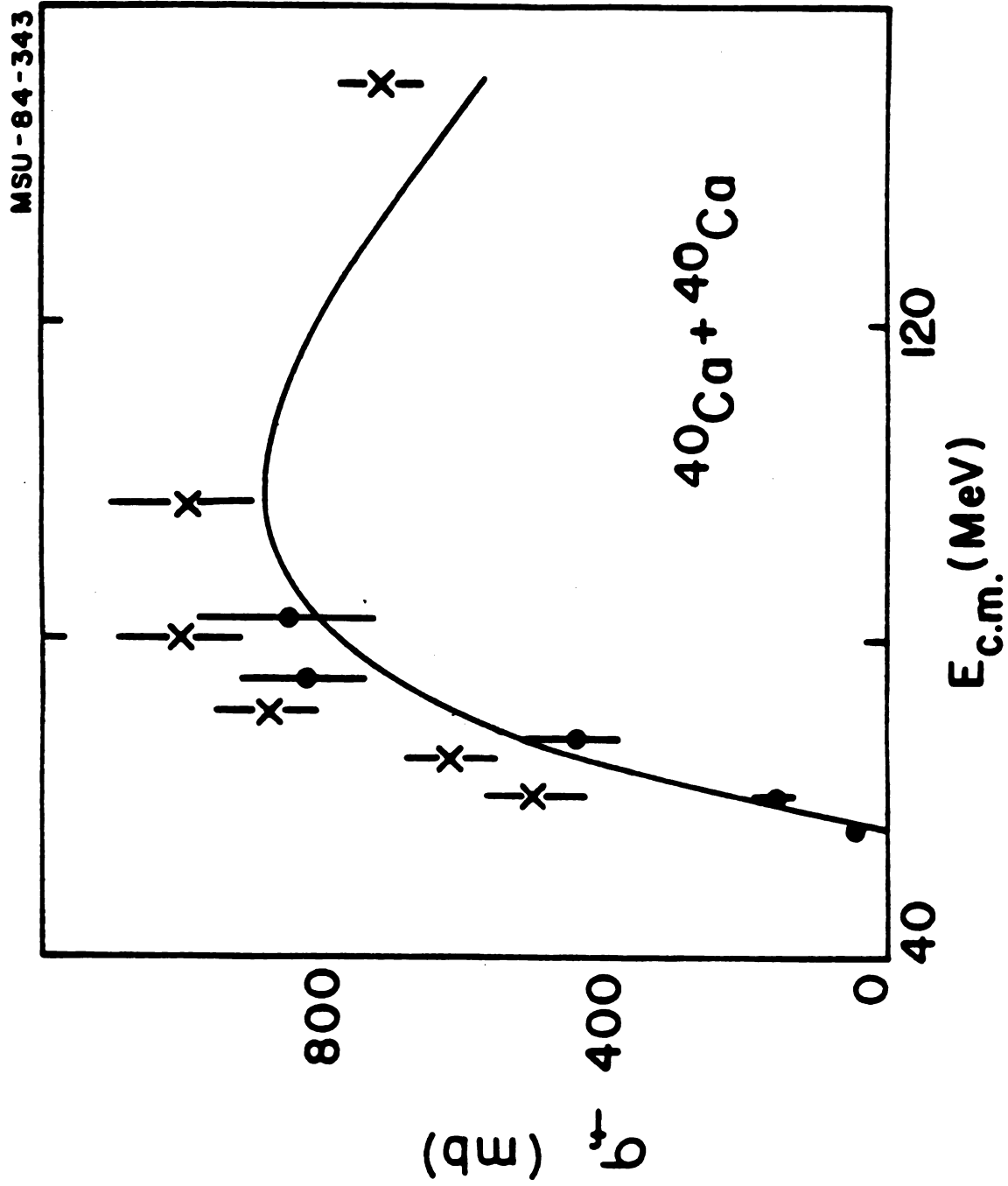


Figure 3.3. Fusion cross section versus energy for the system $^{40}\text{Ca} + ^{40}\text{Ca}$. Data points are from Refs. 16 and 17.

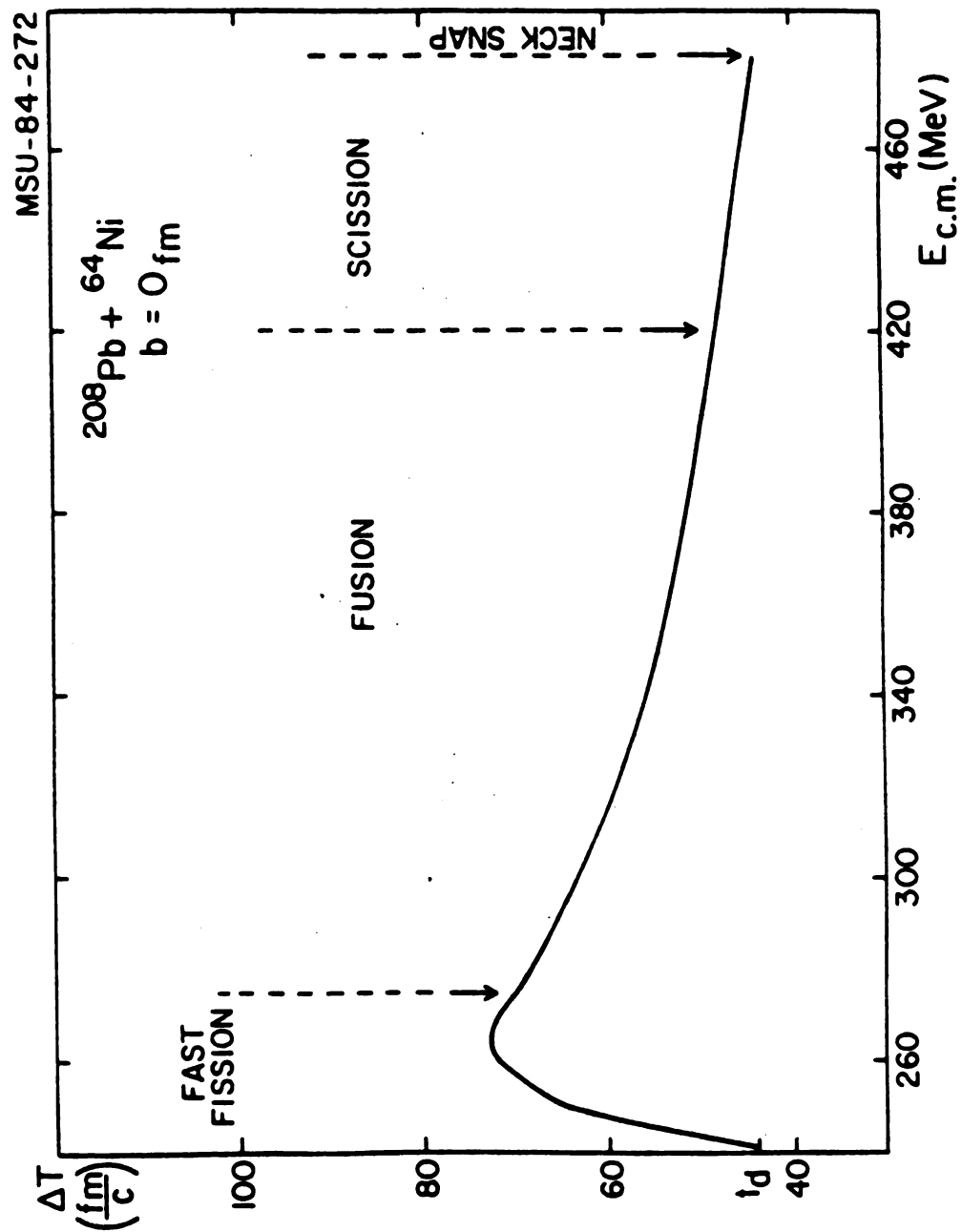


Figure 3.4. Same as Figure 3.2 for the system $^{208}\text{Pb} + ^{64}\text{Ni}$. The time delay t_D is explicitly indicated in the figure.

In general the fusion observed in this region is due to quantum fluctuations. It is very interesting to notice that in the first region the interaction time is very long, of the order of 700 fm/c. This might be a signature for fast fission.

A comparison of this model with experiments performed at GSI using a Pb beam, is shown in fig.3.5a,f [19]. There is an overall good agreement with some discrepancies for the ^{48}Ca target. For impact parameters where fusion is predicted by experiments, we find an interaction time ranging from 500 to 1000 fm/c and this could explain the difference with experiments.

A comparison with experiments performed at MSU is shown in fig 3.6a,b [9,20]. In this case there is a systematic disagreement at higher energies. The interaction time is of the order of 300 fm/c and this suggests that the system could have enough time to relax the initial mass asymmetry. This argument is however not sufficient to affirm that the experimental fusion cross section contains a contribution from fast fission. Finally in fig.3.7a,d a comparison of the model with data for different systems is presented [21-25].

3.3 Comparison with Extra Push Model

We showed above how the necessity of an extra energy to get fusion arises quite naturally in our model. This is also a characteristic of Swiatecki's model and it is not surprising since both models are based on one-body dissipation. The main results of the extra push model are confirmed in our picture. A direct comparison between the two models is

Figure 3.5a-f. Fusion cross sections versus energy in the C.M. for different systems. Data points are from Ref. 19.

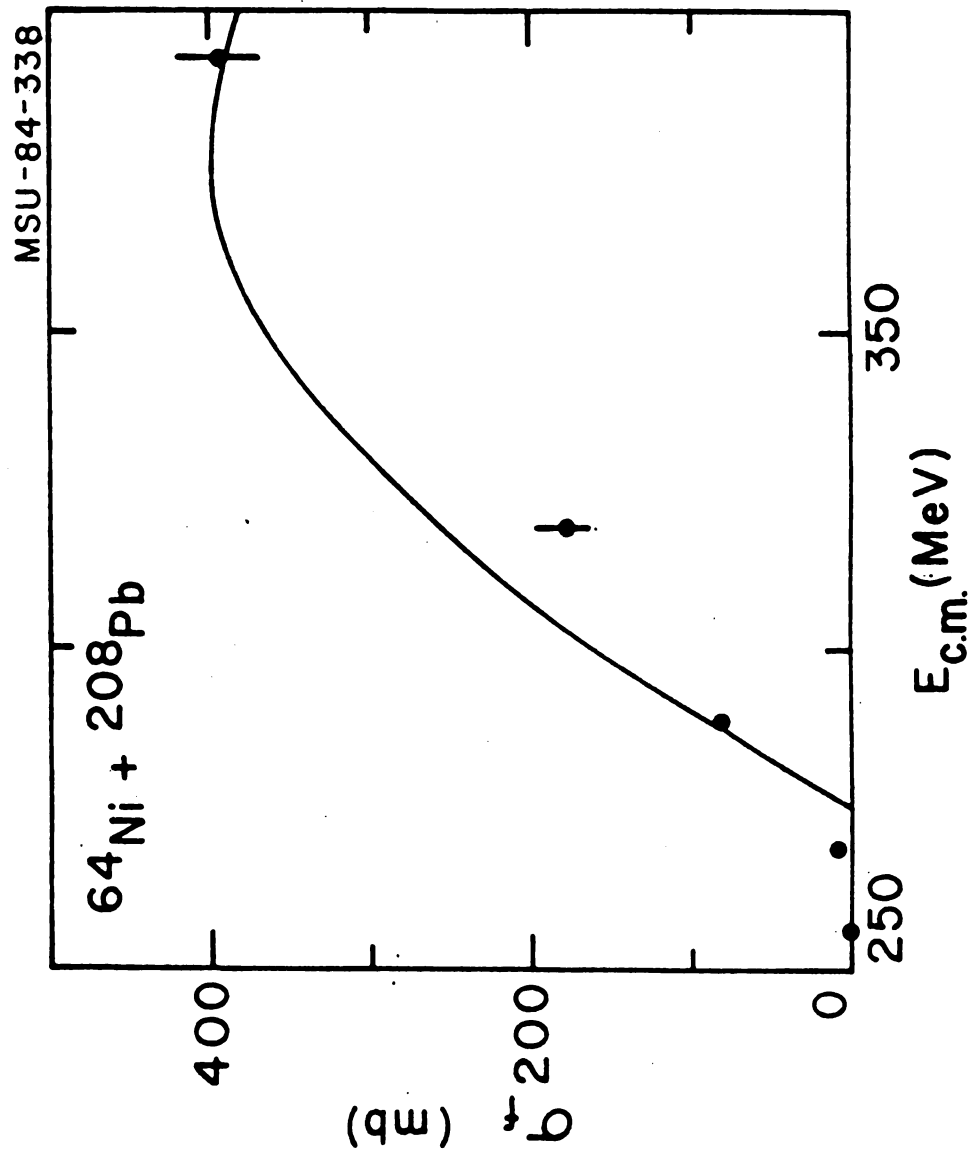


FIGURE 3.5a

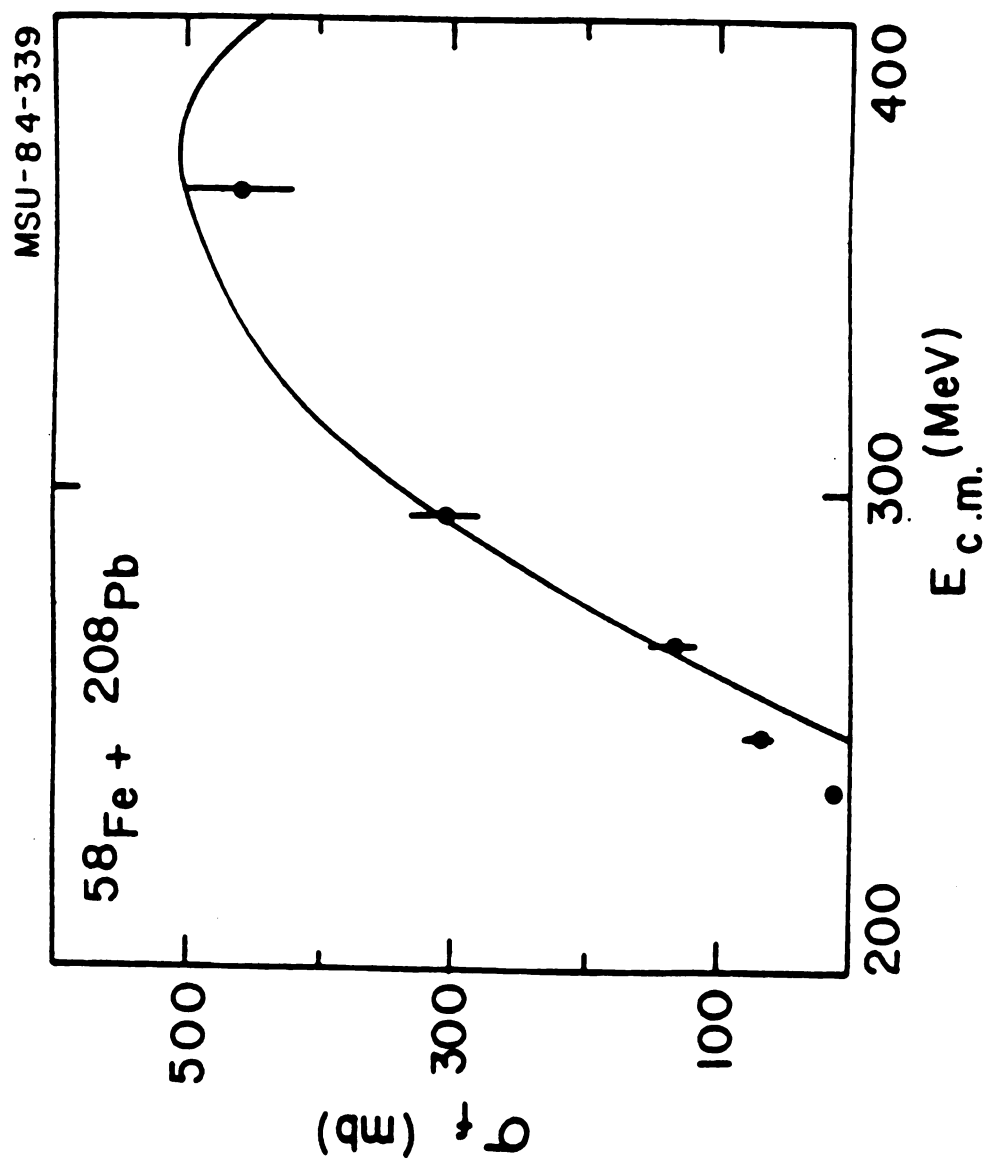


FIGURE 3.5b

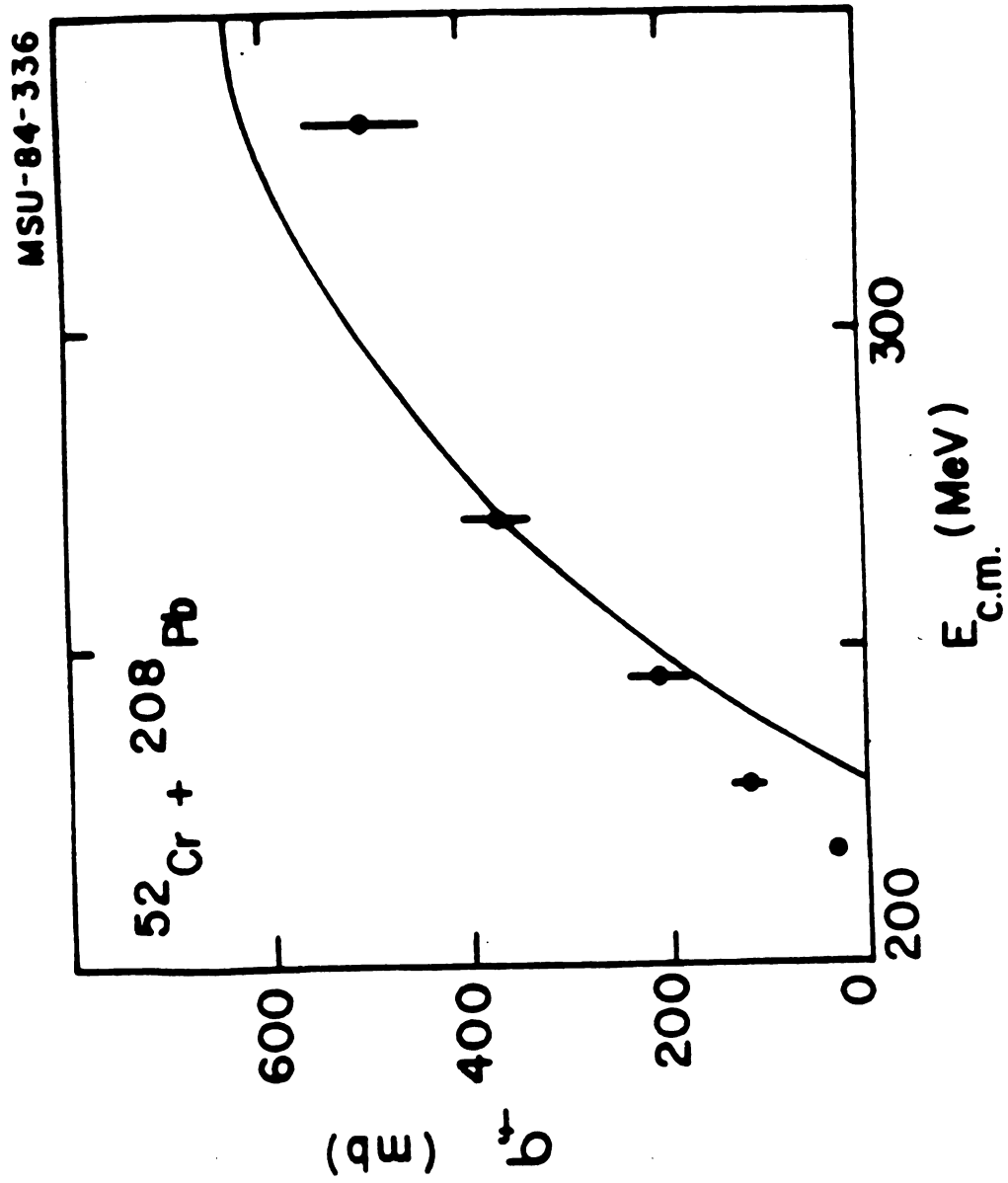


FIGURE 3.5c

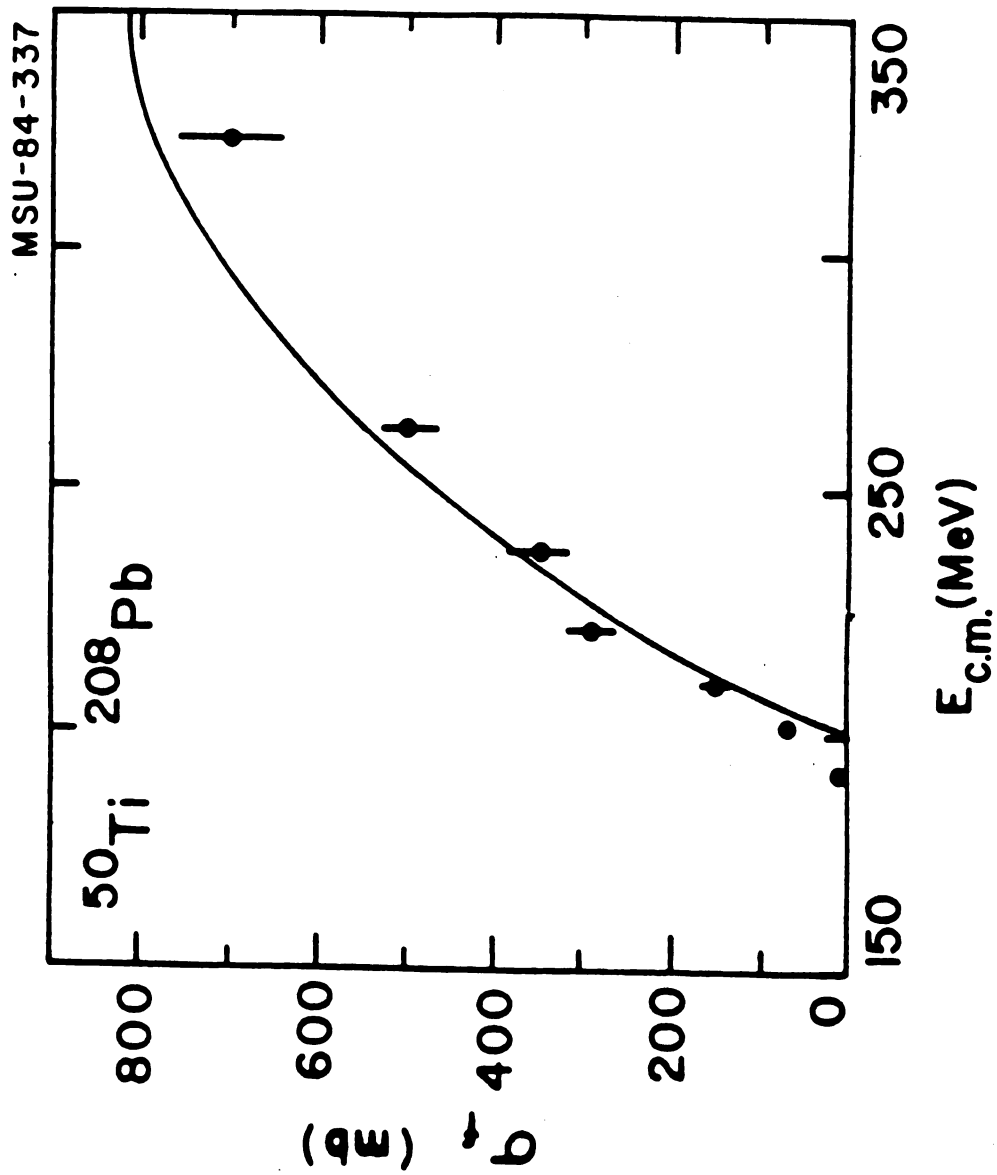


FIGURE 3.5d

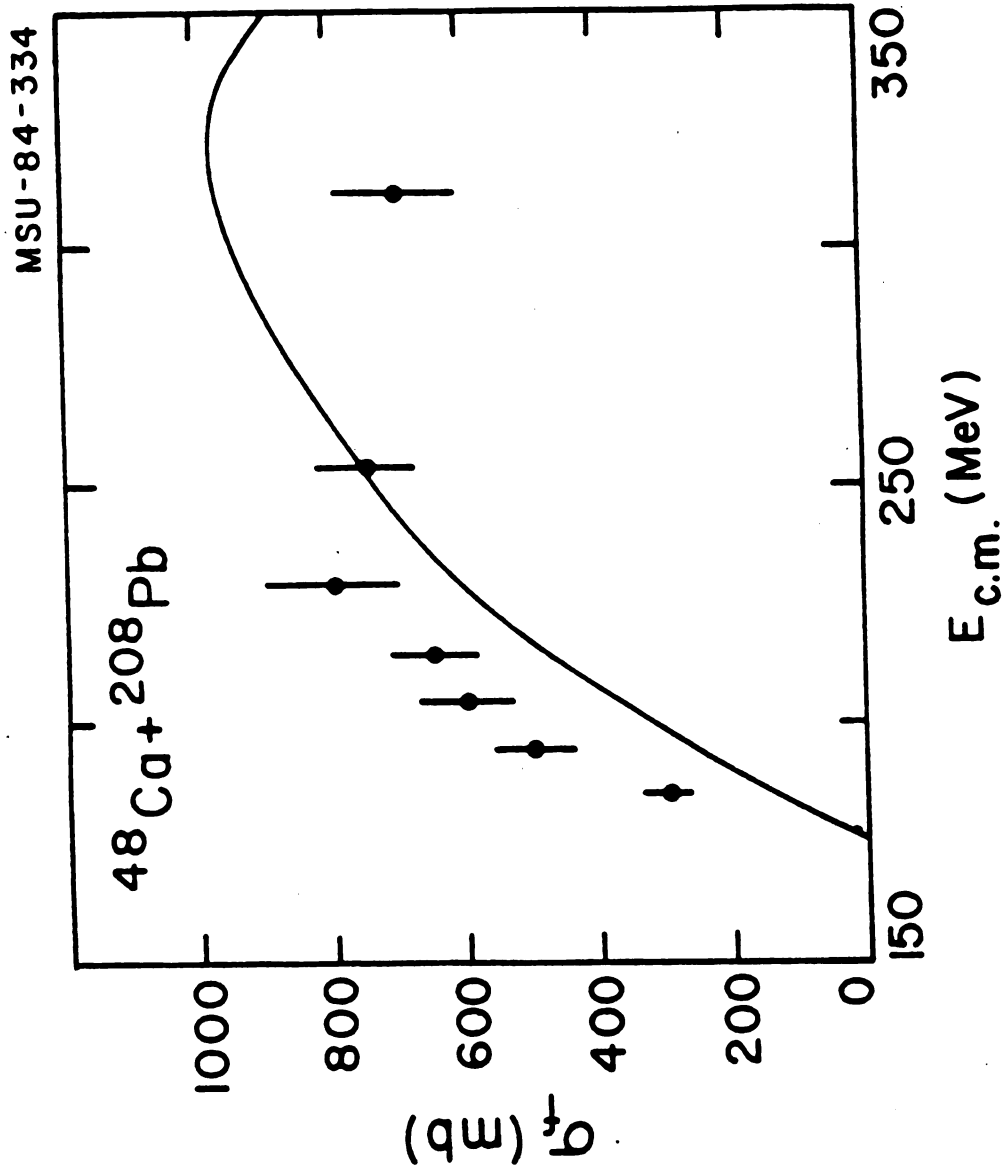


FIGURE 35.e

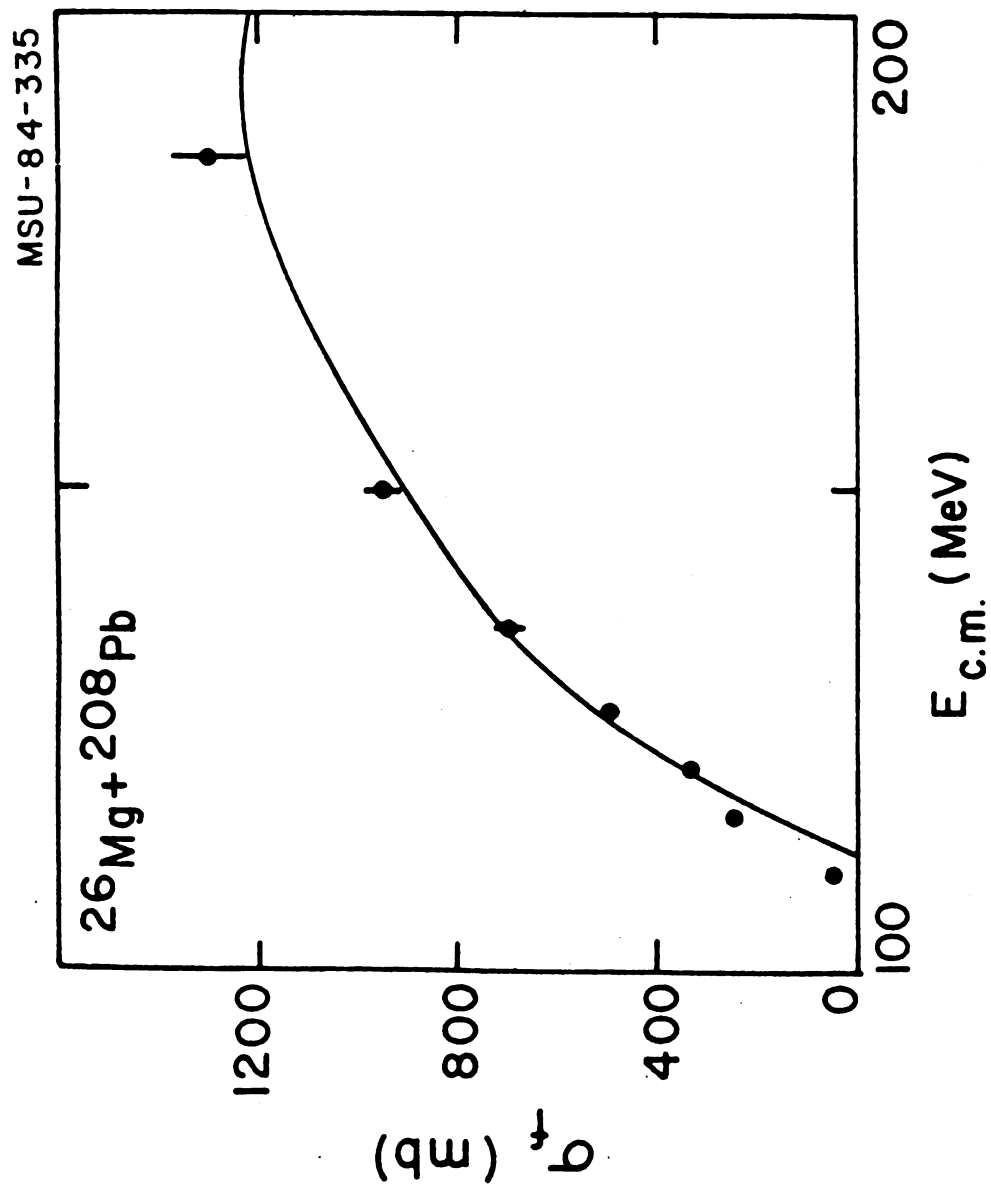


FIGURE 3.5f

Figure 3.6a,b. Same as Figure 3.5. Data are from Ref. 20.

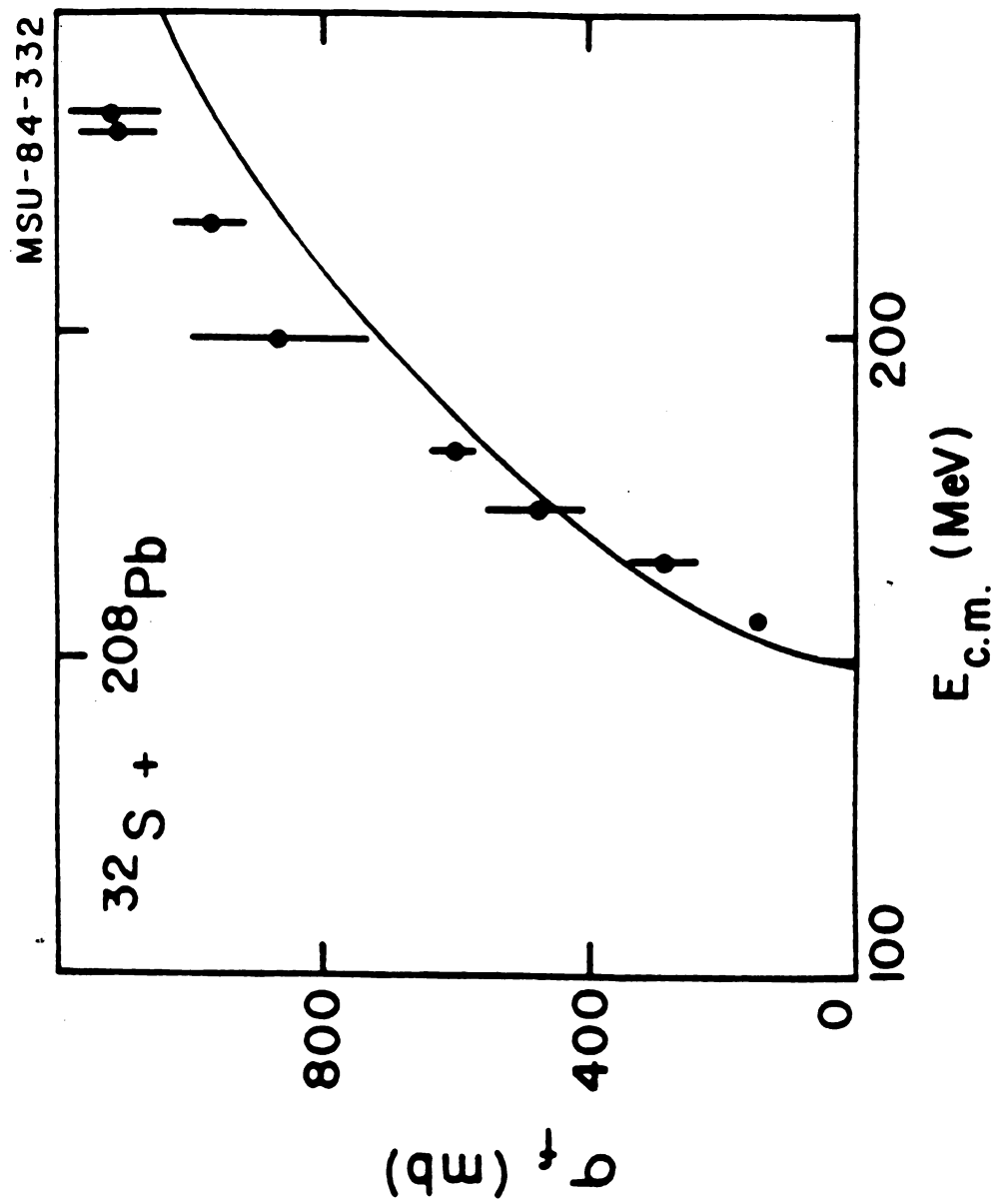


FIGURE 3.6a

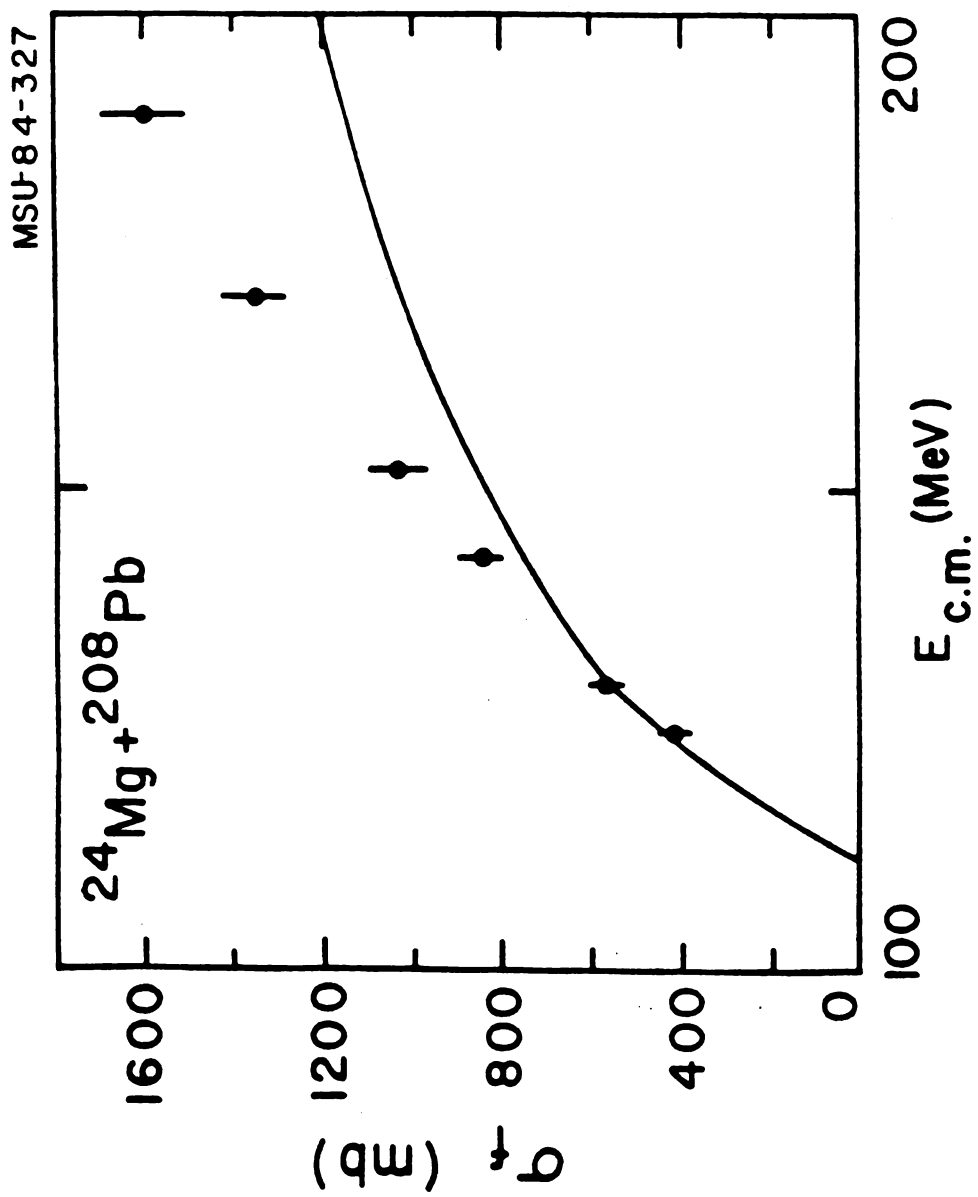


FIGURE 3.6b

Figure 3.7a-d. Same as Figure 3.5. Experimental data are from Refs. 21 through 25.

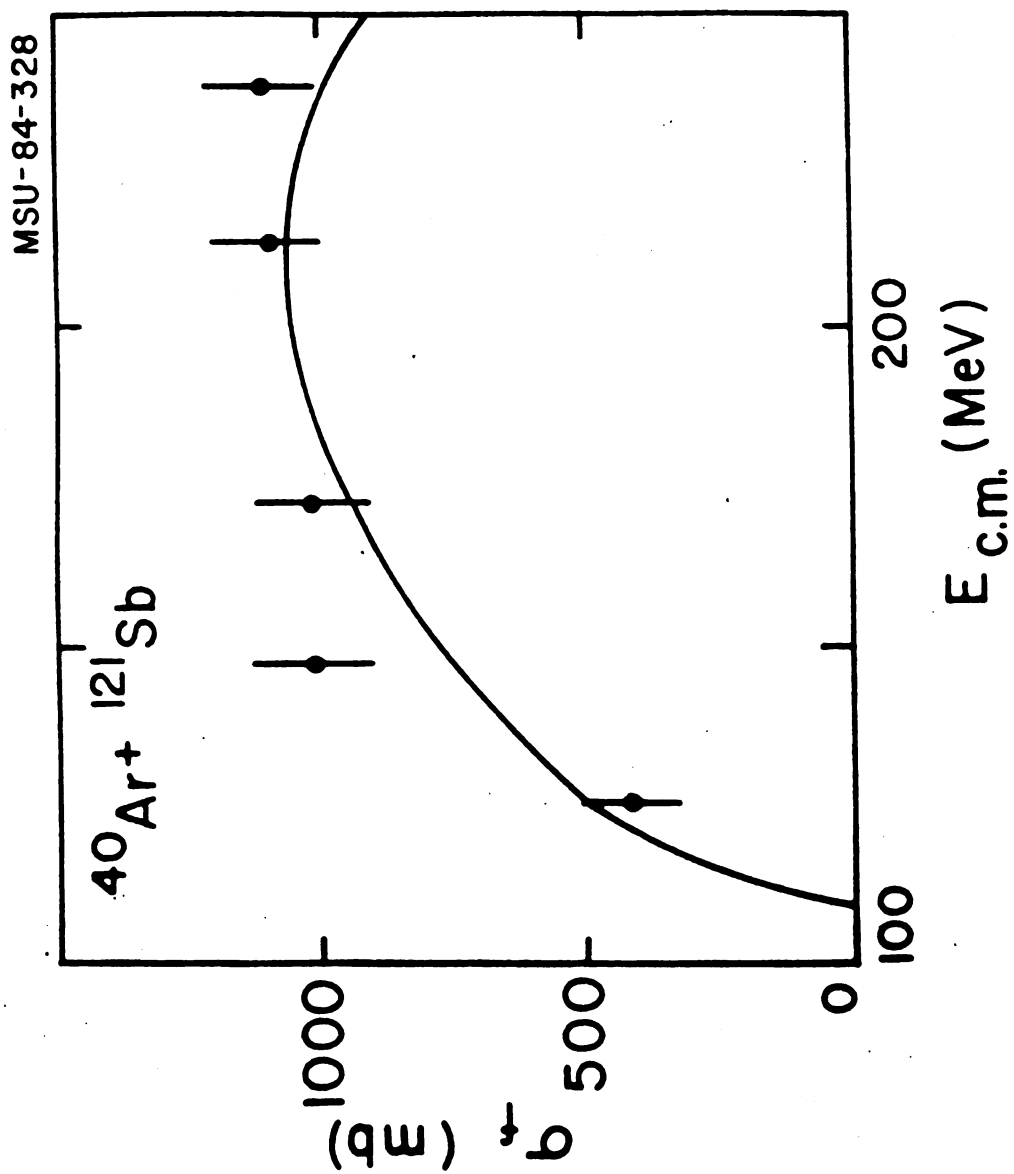


FIGURE 3.7a

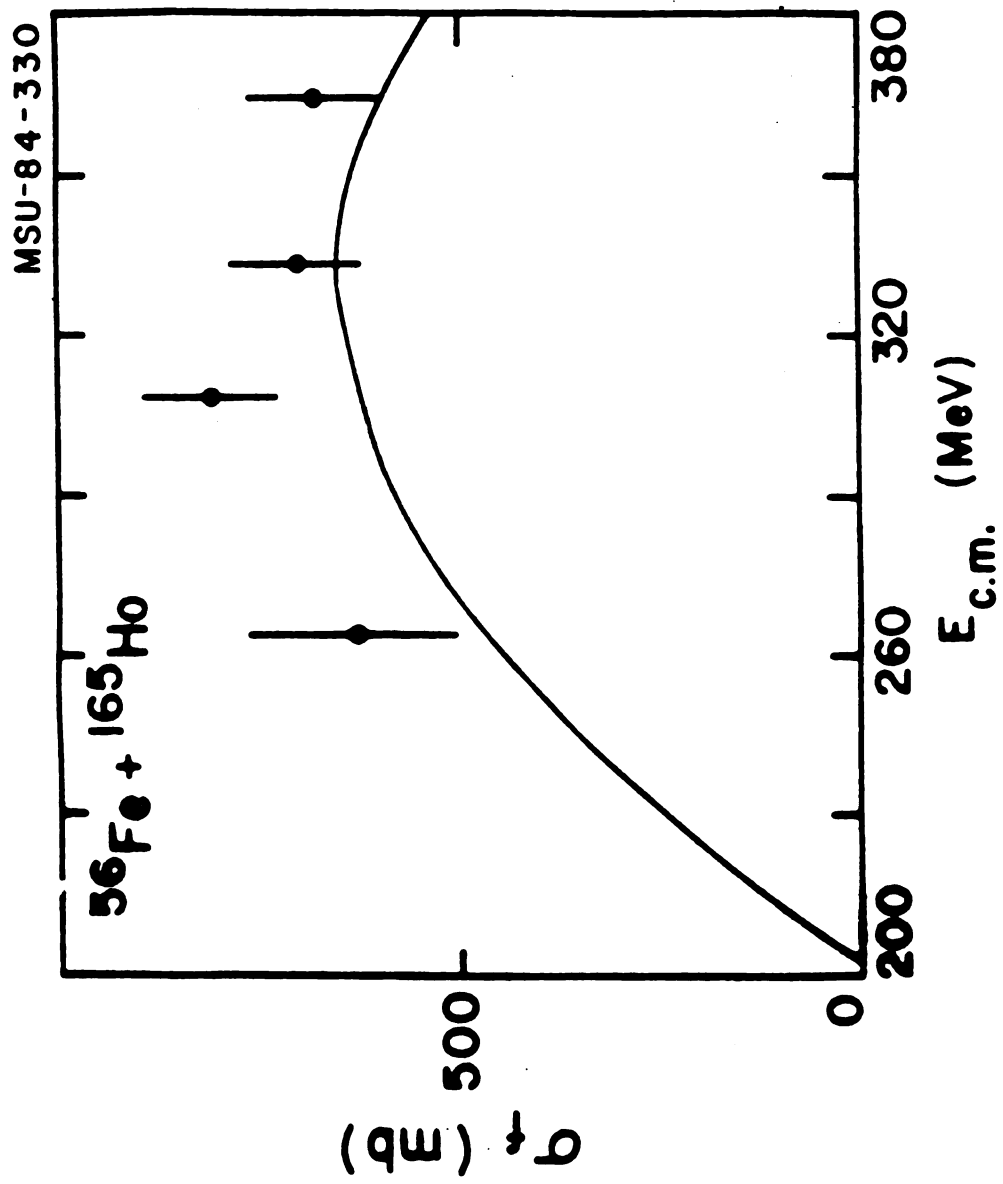


FIGURE 3.7b

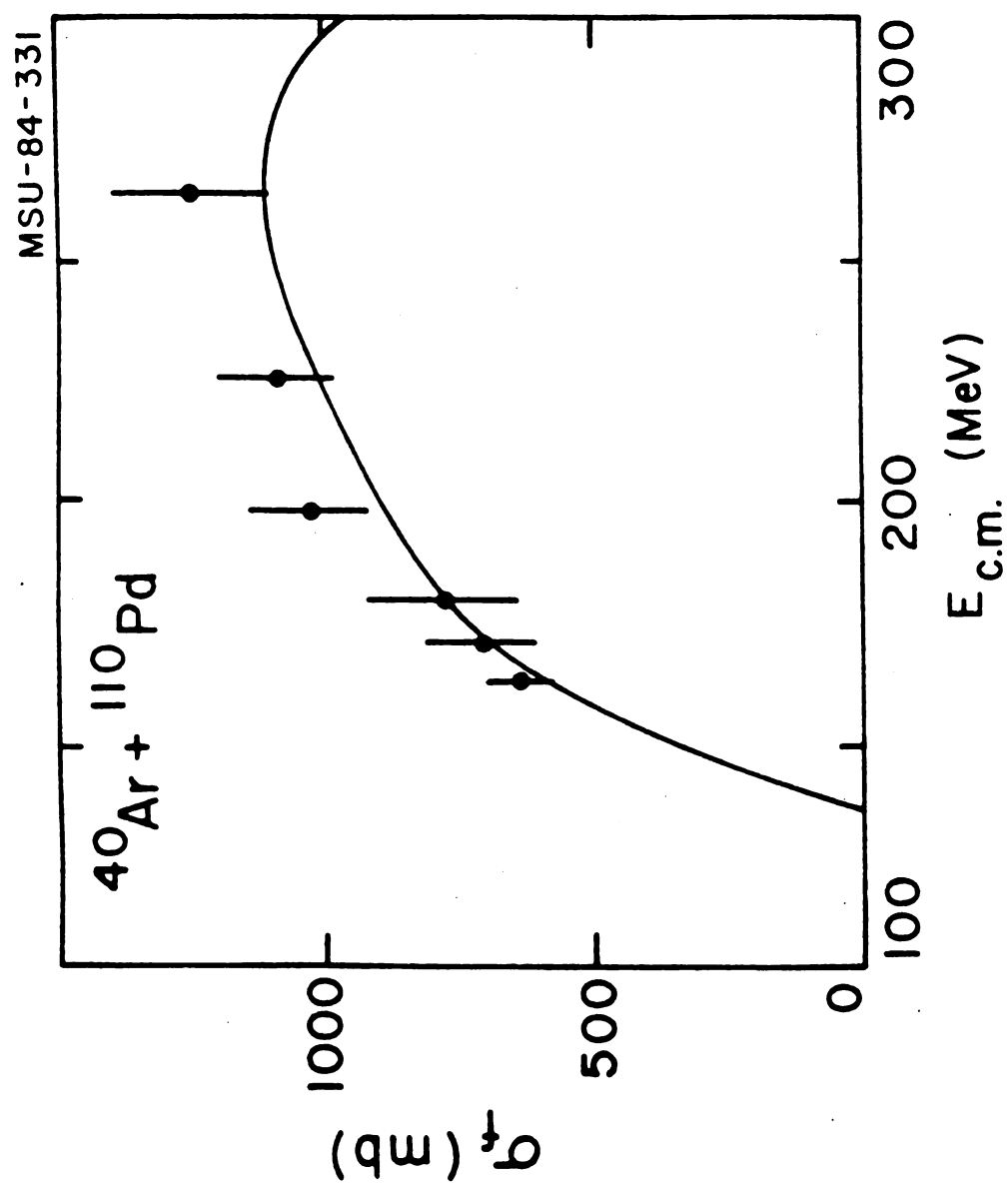


FIGURE 3.7c

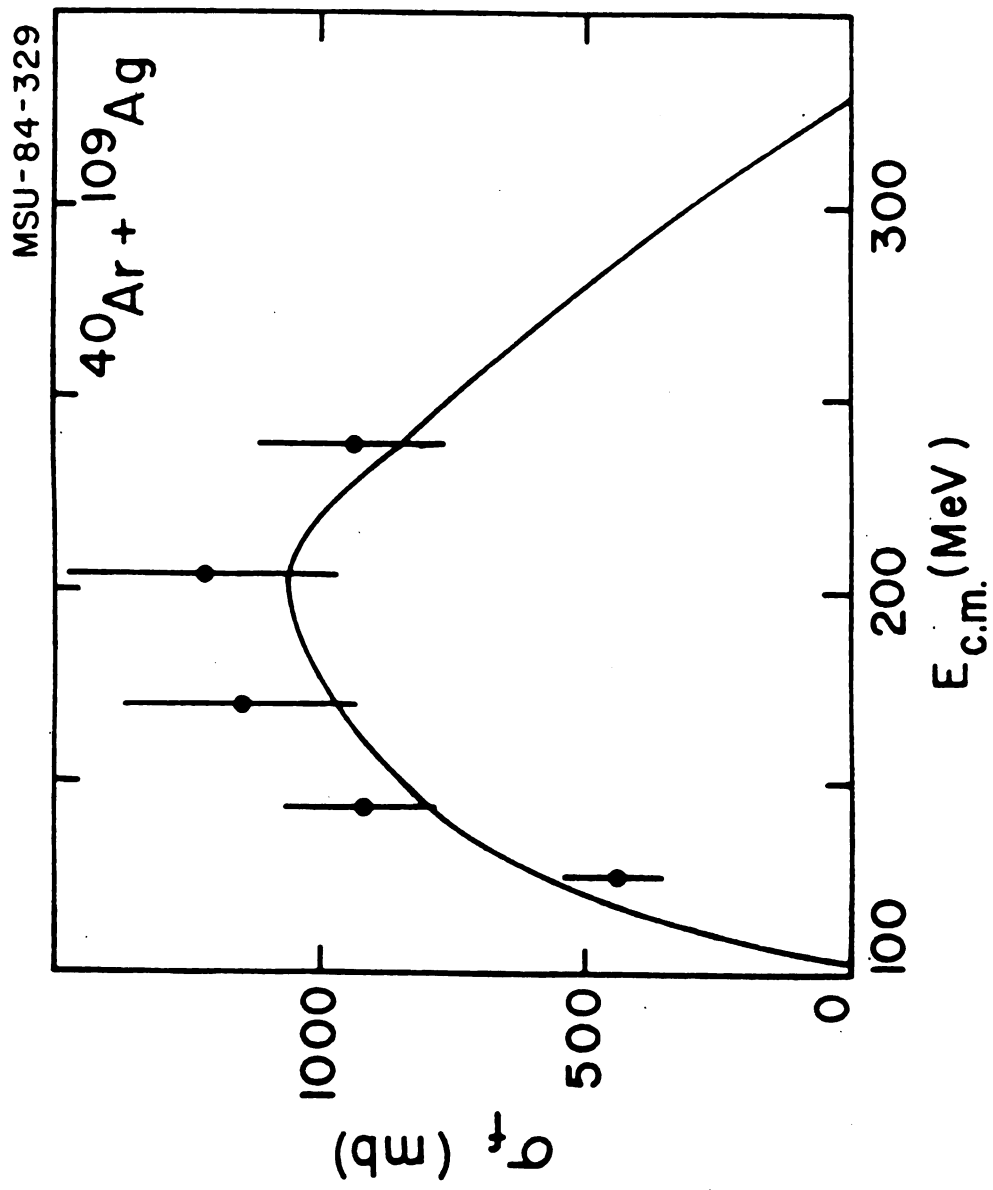


FIGURE 3.7d

done in fig.3.8a,b for systems near the interesting region of superheavy elements. In the first graph the fusion and total reaction cross section is plotted for the system $^{209}\text{Bi} + ^{54}\text{Cr}$ [7,8]. Fusion for this system has been observed at the energies indicated by the arrows [32]. The Bass and proximity potentials give the same predictions for the total reaction cross section and therefore the slight discrepancies in the fusion region are due to other reasons. The same agreement is found for the reaction $^{248}\text{Cm} + ^{48}\text{Ca} \rightarrow ^{296}\text{X}$.

This reaction is very interesting because the compound nucleus has a neutron number close to the magic $N=184$ and it should be possible to detect experimentally.

Figure 3.8a,b. Reaction (full line) and fusion cross sections (dashed line) calculated using the present model, compared to the results of the "extra-push" model (dots and squares, respectively), Refs. 7 and 8.

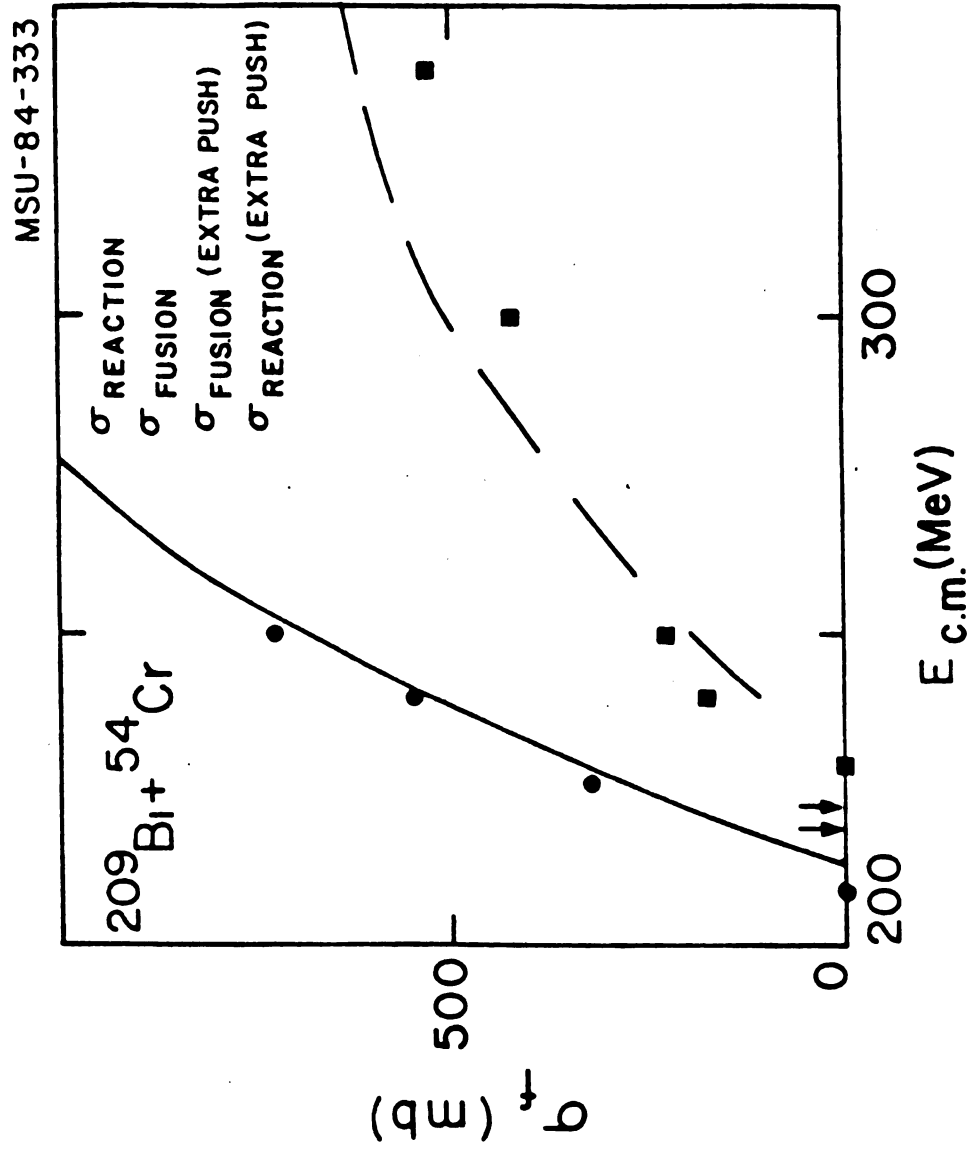


FIGURE 3.8a

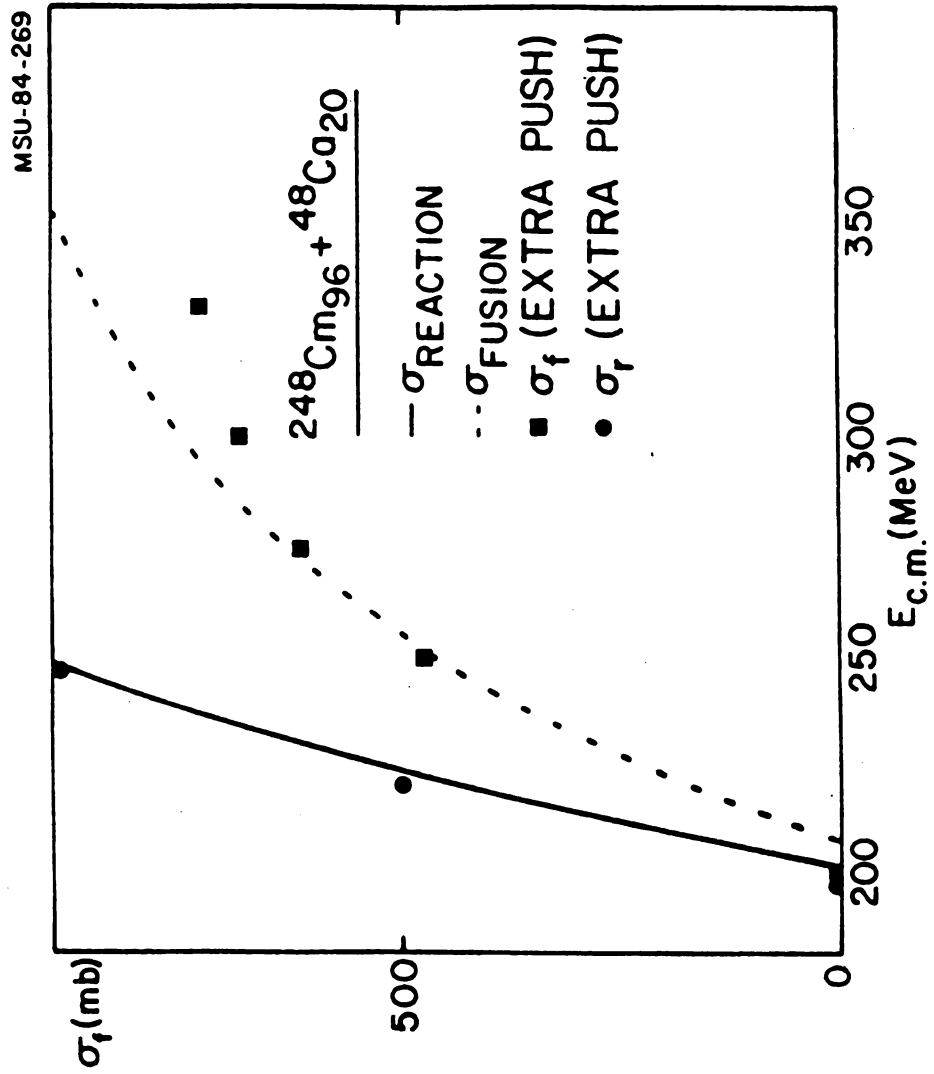


FIGURE 3.8b

Chapter IV

4.1 Deep Inelastic Reactions

The very nature of the damping mechanism in heavy ion collision is still an open problem. The good agreement of our model with experimental fusion cross sections gives support to the concept of one-body dissipation. We expect two-body dissipation to become more and more important when the beam energy is increased.

The dominant process in the high energy region is the deep-inelastic reaction. Its main feature is the great energy loss, which suggests that the nuclei are strongly elongated in the exit channel. This occurs in our model and we showed this explicitly in fig.2.1. The large elongation of the two nuclei implies that they have a long interaction time. A large number of nucleons are exchanged between the two nuclei. The longer the system remains in contact, the more mass and charge is exchanged. The upper limit of this process is when the combined system fissions symmetrically. This case is very similar to fission following fusion but with a shorter interaction time (fast-fission). Therefore the angular distribution is not strictly symmetric in the C.M. system and can be distinguished experimentally.

We saw in the preceding chapter that fast fission occurs in our model for heavy nuclei in the extra push energy region and for high angular momenta. These features have also been seen in TDHF [10]. We can think

of fast fission as the border between fusion and deep-inelastic scattering.

At higher energies or angular momenta the interaction time becomes very short and preequilibrium processes occur. The main feature in this case is the emission of light particles in the early stage of the reaction. These particles are essentially neutrons and protons (Promptly Emitted Particles or Fermi jets), and for very high energy ($>10\text{MeV/u}$), also α particles or even bigger nuclei [26,4].

4.2 Comparison with Experimental Data

In fig.4.1 we plot the energy spectra for the system $^{84}\text{Kr}+^{209}\text{Bi}$. The peak at zero energy loss is due to quasielastic scattering. At higher energy there is a broad peak due to deep-inelastic scattering. Our model gives the correct position for the peaks but the magnitude of the cross section is overestimated. This is a limit of any classical model: stochastic processes broaden all sharp structures. At medium energy losses the experimental data are underestimated. In this region of energy losses the nuclei are strongly elongated and there is a large mass transfer. Damping of mass asymmetry becomes important and should explain the discrepancy.

Our model is in complete disagreement with experiments for the highest values of energy losses. At angular momenta close to the grazing value, the systems have a short interaction time and the neck snaps. This rapid process might result in more than two particles in the exit channel and this would explain the discrepancy.

A clear evidence of direct fragmentation into more than two nuclei has been observed for the reactions $^{32}\text{S}+^{58}\text{Ni}$ and $^{35}\text{Cl}+^{58}\text{Ni}$ at energies

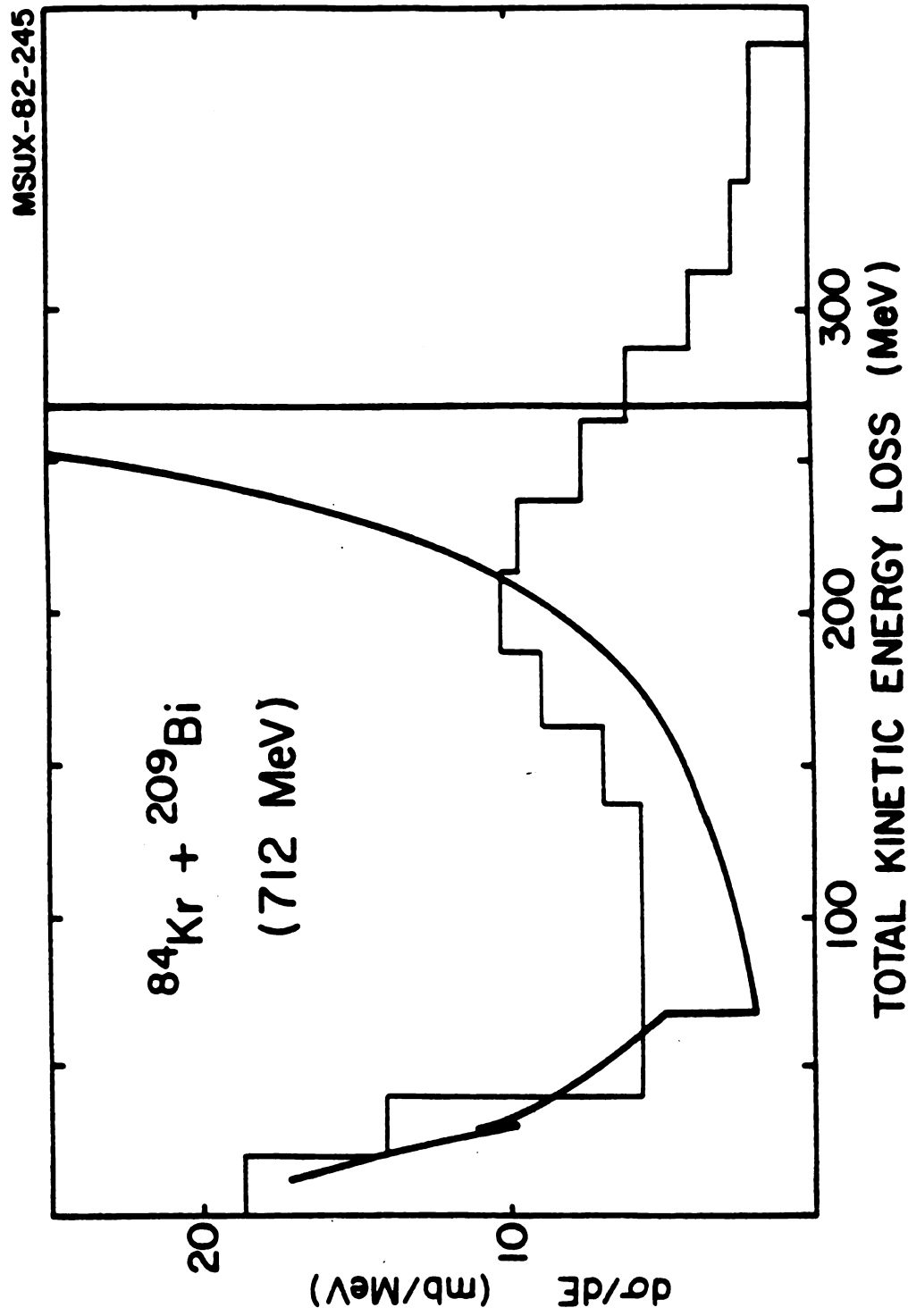


Figure 4.1.1. The energy loss spectrum for the system $^{84}\text{Kr} + ^{209}\text{Bi}$ at $E_{\text{LAB}} = 712$ MeV.

above 10 MeV/u. The experimental data suggest that all three fragments are emitted in one step [4].

These features are confirmed from TDHF studies. For the system $^{136}\text{Xe}+^{209}\text{Bi}$ at 8.3 MeV/u, a three body break-up was observed [27]. At this relatively low energy the emission of an α -like fragment from the neck at scission occurs only at high angular momentum ($l=100\hbar$). At energies of about 13MeV/u a prompt emission of nucleons is observed for the system $^{16}\text{O}+^{93}\text{Nb}$ [28]. A classical model was also proposed to predict the Fermi jet's behavior [26]. The basic idea is that the nucleons in passing through a window from one nucleus to the other, acquire a new velocity which is the sum of the relative velocity plus the Fermi velocity. Thus if the kinetic energy of the nucleon in nucleus B is enough to overcome the nuclear barrier (plus the Coulomb if it is a proton), it will leave the system. This process can be calculated in our model since it explicitly treats the neck's evolution. But it has the same drawback as in the original model, namely the energy threshold for Fermi jets is half the value predicted in TDHF. This problem needs further investigation.

In conclusion let us discuss the results of a recent experiments on the $^{58}\text{Ni}+^{58}\text{Ni}$ and $^{58}\text{Ni}+^{197}\text{Au}$ systems at 15 MeV/u [29]. The purpose of this experiment was to check if thermal equilibrium is attained during the reaction. If this is true, we expect the available excitation energy to be shared in proportion to the masses of the projectile and the target.

For the system $^{58}\text{Ni}+^{197}\text{Au}$, the experimental angle-integrated charge distributions show a strong drift of the charge centroids away from symmetry. The light particle evaporation can be calculated under the

hypothesis of thermal equilibrium. The values of the predicted charge centroids are larger than those observed. If the excitation energy is assumed to be shared equally between the two fragments, rather than according to the masses, the observed charge distributions are reasonably described. This conclusion is checked for the system $^{58}\text{Ni} + ^{58}\text{Ni}$. Since the system is symmetric we expect an evaporation calculation to reproduce the experimental results. This is indeed the case.

An explanation of the nonthermal energy sharing is that at high bombarding energy, the system does not have enough time to reach thermal equilibrium. In fig. 4.2 we show the variation of the interaction time and the energy loss with impact parameter. The maximum value for the energy losses agree with the experimental observation. The interaction time is very short, of the order of 10^{-22} sec. This implies a sudden rupture of the neck and the possibility of a three body process in the exit channel. The same considerations can be repeated for the system $^{56}\text{Fe} + ^{165}\text{Ho}$ at 8.5 MeV/u. At this lower energy, the centroids of the charge and neutron distributions are well described by assuming a smooth transition from the limit of equal sharing of the dissipated energy occurring at small energy loss, to the limit of equal temperature at large energy loss. In fig. 4.3 we plot the interaction time and energy loss versus impact parameter. For b less than 4.6 fm we get fusion. The fusion cross section is 665 mb which agrees nicely with experimental data. At higher impact parameters, our model gives a very long interaction time, of the order of 10^{-21} sec. In this case the system has enough time to reach thermal equilibrium. For the highest values of impact parameters, the interaction time is equal

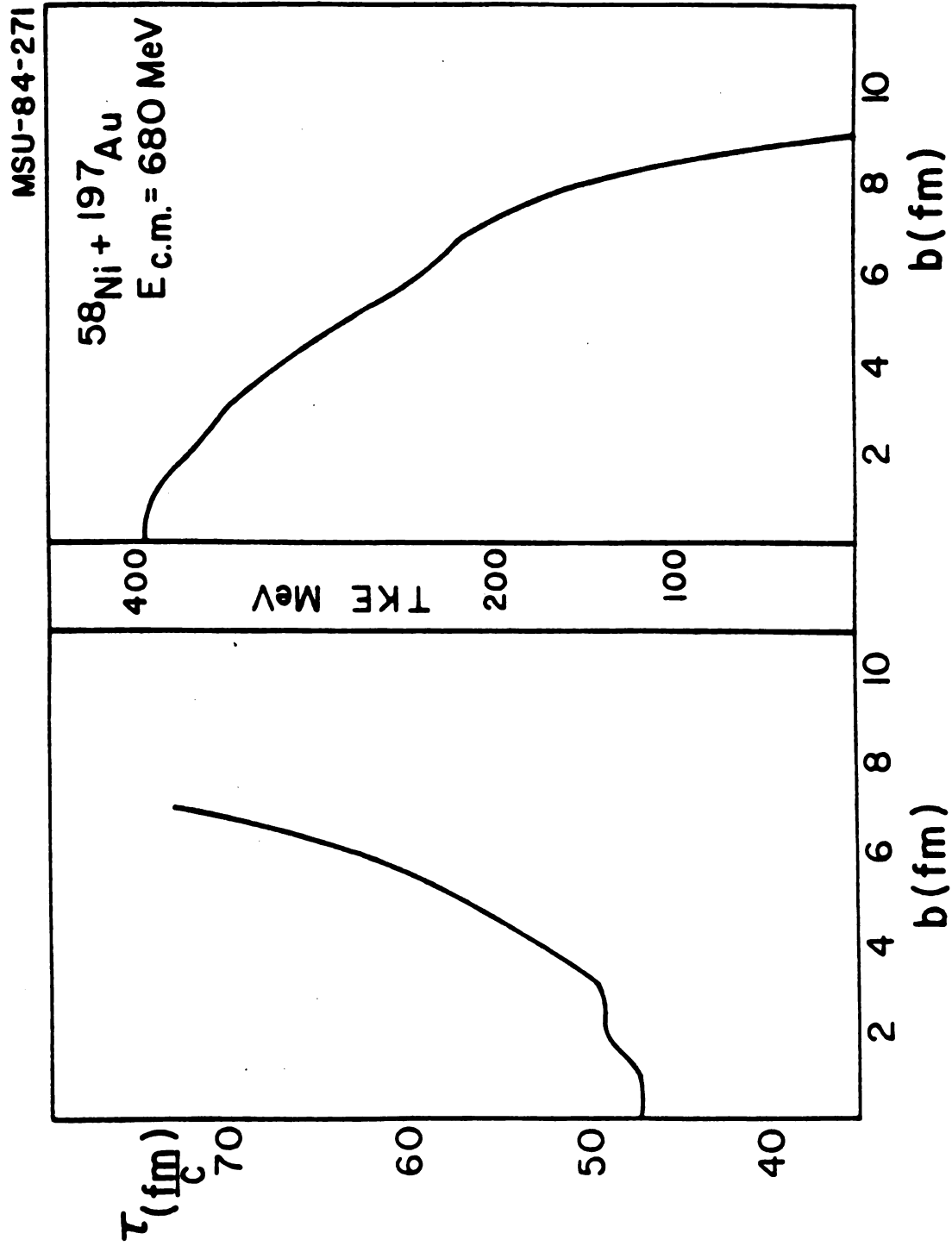


Figure 4.2. Interaction time and energy loss versus impact parameter for the system $^{58}\text{Ni} + ^{197}\text{Au}$.

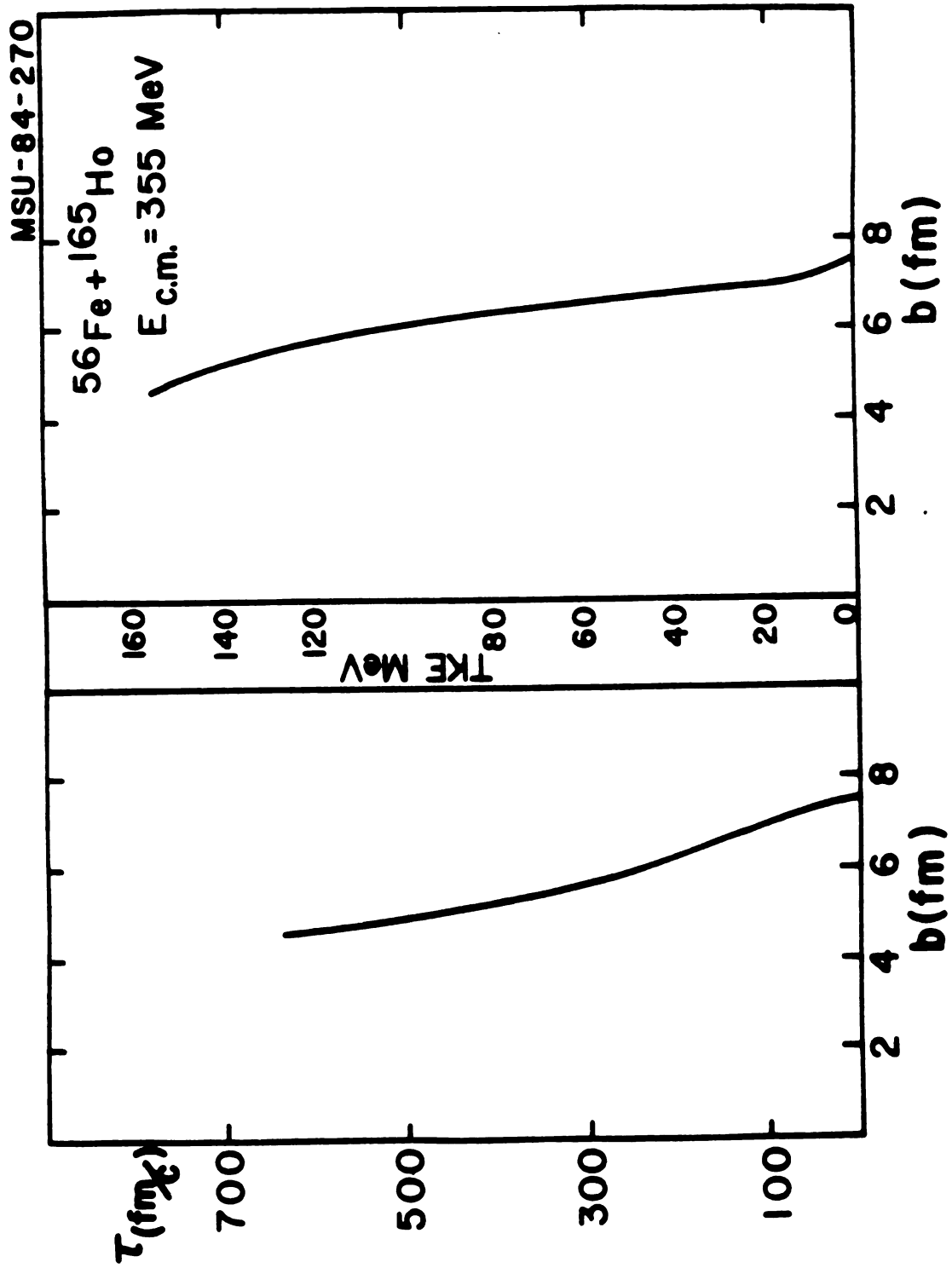


Figure 4.3. Same as Figure 4.2 for the system $^{56}\text{Fe} + ^{165}\text{Ho}$.

to that for the system $^{58}\text{Ni} + ^{197}\text{Au}$, resulting in a preequilibrium process. Therefore it is not surprising that the best description of the data is given by a smooth transition as described above.

Our model suggests that the time the system takes to reach equilibrium is surely larger than 50 fm/c and smaller than 300 fm/c. Bertsch has determined the local equilibrium time by considering the equilibration of a quadrupole deformation of the Fermi sphere within the Fermi-gas approximation [30]. His numerical result is in good agreement with the above estimate.

APPENDIX

HEAVY-ION DYNAMICS IN A TDHF-BASED CLASSICAL DESCRIPTION

Aldo Bonasera

Research Institute for Fundamental Physics,
Kyoto University, Kyoto 606, Japan and
Cyclotron Laboratory, Michigan State University,
East Lansing, MI 48824, USA*

Abstract:

We present a simple classical model based on the mean-field theory. This model is in reasonable agreement with trends in fusion cross-sections for heavy nuclei, including the barrier to fusion at high Z^2/A . A critical value of the interaction time, which leads to fast fission, is estimated from the reaction $^{238}\text{U} + ^{89}\text{Y}$ at $E_{\text{lab}} = 6$ MeV/u. Finally, we estimate the equilibration time for energy by comparing the TDHF-based classical model with recent-experimental data.

1. Introduction

In this contribution we investigate low-energy heavy-ion collisions using a simple classical model. This model is based on the dynamics of Time-Dependent Hartree-Fock (TDHF) theory which at present seems to be the best theory at the microscopic level. Unfortunately, the TDHF theory presents serious computational difficulties and sometimes the results are in disagreement with experimental data.⁵⁾ Our purpose is to reduce the mean-field theory to classical equations of motion, which can be easily solved.

This work is organized in the following way. In section 2 we discuss the equations of motions. In section 3 the results are compared with experimental data on fusion and deep inelastic scattering. Collision times are calculated for a variety of reactions and we estimate a critical value for the interaction time which leads to fast fission and is common to all systems.⁴⁾ Also, Comparison with the results of a recent experiment⁶⁾ suggests that the equilibration time for energy lies between 50 fm/c and 250 fm/c. We summarize our main results in section 4.

2. Equations of Motion

A convenient way to reduce the TDHF system to a classical form is by taking its Wigner Transform. In the limit $\hbar \rightarrow 0$, this gives the Vlasov equation

* Present address.

$$\frac{d}{dt} f(\vec{r}, \vec{p}, t) = \{h(\vec{r}, \vec{p}, t); f(\vec{r}, \vec{p}, t)\} , \quad (1)$$

where $h(\vec{r}, \vec{p}, t) = \frac{p^2}{2m} + w(\vec{r})$ is the Wigner transform of the self-consistent HF hamiltonian and $f(\vec{r}, \vec{p}, t)$ is the phase-space distribution. The curly brackets indicate Poisson brackets.

Classically, the most important degrees of freedom are the conjugate variables \vec{r} and \vec{p} describing the relative motion of the two nuclei. We define these quantities as

$$\begin{pmatrix} \vec{r} \\ \vec{p} \end{pmatrix} = \int_A d\vec{r} d\vec{p} \begin{pmatrix} \vec{r} \\ \vec{p} \end{pmatrix} f(\vec{r}, \vec{p}, t) - \int_B d\vec{r} d\vec{p} \begin{pmatrix} \vec{r} \\ \vec{p} \end{pmatrix} f(\vec{r}, \vec{p}, t) , \quad (2)$$

where A and B refer to the two colliding nuclei. The Hamilton equations of motion of nucleus A, say, are found by taking the time derivative of eq.(2). Using eq.(1), and after some algebra, we obtain

$$\frac{d}{dt} \vec{r}_A = \frac{\vec{p}_A}{m} \quad (3)$$

and

$$\frac{d}{dt} \vec{p}_A = \pi r_N^2 \hat{n} \cdot [\vec{\tau} + \vec{l} \nabla \left(\frac{\partial U}{\partial p} - U \right)]_{NM} + 2\pi\sigma r_N \hat{n} + \text{Coulomb term} ,$$

where r_N is the radius of the neck³⁾ formed during the reaction, σ is the surface energy²⁾, and we assume that $U(\vec{r}) \equiv \int d\vec{p} w(\vec{r}) f(\vec{r}, \vec{p}, t)$ is a local function of the density. The subscript NM denotes a nuclear-matter approximation. The particle-flux tensor $\vec{\tau}$ was evaluated by Randrup.⁷⁾ We modify his prescription by introducing a time delay in the damping term.³⁾

Before the nuclei touch the dynamics is well described by potential models and we shall use the Bass potential in calculations.⁸⁾

Finally, we shall assume that the two nuclei separate into two fragments again in the rebounding phase if $r_N < 1$ fm or a critical velocity for neck snap is exceeded¹⁾.

3. A Comparison with the Experimental Data

For light nuclei, the reaction cross-section at energies just above the Coulomb barrier is dominated by the fusion cross-section. For very heavy

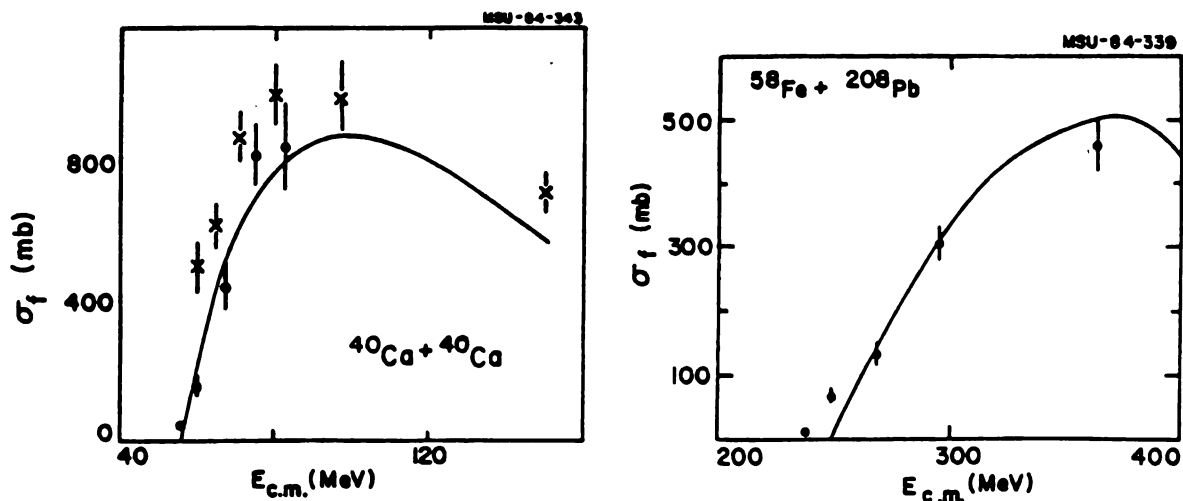


Fig.1. Fusion cross-section versus energy in the C.M. for the systems $^{40}\text{Ca} + ^{40}\text{Ca}$ 10) and $^{58}\text{Fe} + ^{208}\text{Pb}$ 11)

systems, on the other hand, the Coulomb repulsion is very strong, and the condition that the nuclei touch is not sufficient to cause fusion. Thus, an extra injection energy⁹⁾ is needed in order to produce fusion. These features are well reproduced by our model.³⁾ In fig.1 we show how our model compares with experimental data on fusion cross-sections for the systems $^{40}\text{Ca} + ^{40}\text{Ca}$ 10) and $^{58}\text{Fe} + ^{208}\text{Pb}$ 11). A more detailed comparison with data on fusion cross-sections for several different systems is given in ref.3.

Recently an interesting new phenomenon, called fast-fission, has been observed. Its characteristics are intermediate between fusion and deep inelastic collisions. In this case the binary fragmentation of the intermediate composite system is similar to the fission following complete fusion but with a shorter interaction time.

We estimate a critical value for the interaction time for fast fission⁴⁾ by comparing our model with the recent experimental data obtained at G.S.I. using a ^{238}U beam¹²⁾ incident on several different targets, ranging from ^{16}O to ^{89}Y .

For heavy systems the fusion cross-section is defined as

$$\sigma_{\text{fusion}} \equiv \sigma_{\text{compound nucleus}} + \sigma_{\text{fast fission}} \quad (4)$$

For the system $^{89}\text{Y} + ^{238}\text{U}$ at energy $E_{\text{lab}} = 6 \text{ MeV/u}$, the experimental fusion cross-section is less than 60 mb. Our classical model gives no contribution from compound-nucleus formation. If we assume that interaction times larger than

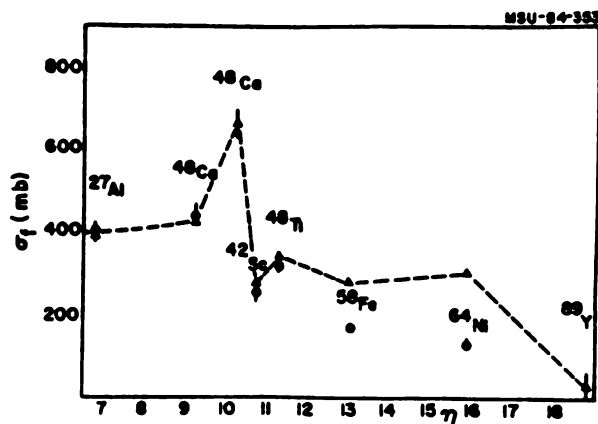


Fig.2. Theoretical fusion cross-section (triangles) versus $\eta = (Z_T^2/A_T)E_{cm}/V_B$ (see text). The different targets are explicitly indicated. The experimental data is from ref.12. The dashed lines are drawn in order to guide the eye.

8×10^{-22} sec lead to fast fission, then we obtain a value for the fusion cross-section in agreement with the observed value. This critical value of the interaction time is independent of the system involved, as we show in fig.2 where the fusion cross-section versus the quantity $\eta = (Z_T^2/A_T)E_{cm}/V_B$ is plotted. Z_T and A_T refer to the charge and the mass of the target, respectively, and V_B is the Coulomb barrier. A comparison of our classical model with other experimental data provides further evidence for the existence of a critical interaction time for fast fission.⁴⁾

The dominant process at higher energies is the deep inelastic scattering. As an example of this type of reactions, we discuss the result of a recent experiment on the systems $^{58}\text{Ni} + ^{58}\text{Ni}$ and $^{58}\text{Ni} + ^{197}\text{Au}$, at 15 MeV/u.⁶⁾ The purpose of this experiment was to see if thermal equilibrium is attained during the reaction. If this is true, then we expect the available excitation energy to be shared between the two nuclei in proportion to the masses of the projectile and the target. The experimental values of the distributions of charge and mass, however, are in agreement with a calculation performed assuming that the energy is shared equally between the two fragments.

One possible explanation of the non-thermal partitioning of excitation energy is that at high bombarding energy, the system has too little time to

reach thermal equilibrium.³⁾ In fig.3 we show how the interaction time and the energy loss vary with impact parameter. The maximum value for the energy loss agrees with the experimental observation. The interaction time is very short, of the order of 10^{-22} s.

The same considerations can be applied to the system $^{56}\text{Fe} + ^{165}\text{Ho}$ at 8.5 MeV/u. At this lower energy, the experimental values on charge and mass distributions agree with calculations performed assuming thermal equilibrium.

In fig. 4 we plot the interaction time and energy loss versus impact parameter. For b less than 4.6 fm we see fusion. For higher impact parameters, the system has an interaction time of the order of 10^{-21} s, and it can

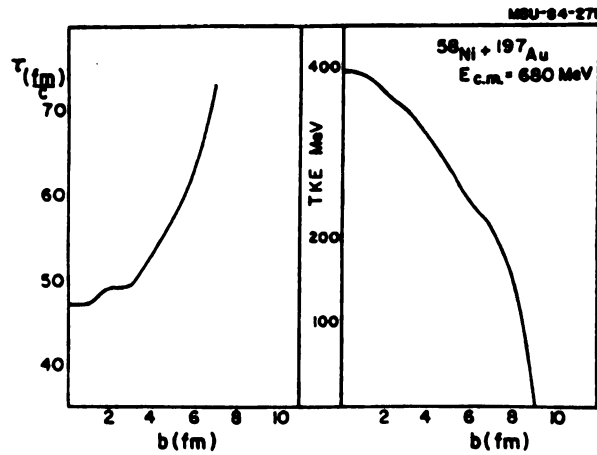


Fig.3. Interaction time and energy loss versus impact parameter for the system $^{58}\text{Ni} + ^{197}\text{Au}$.⁶⁾

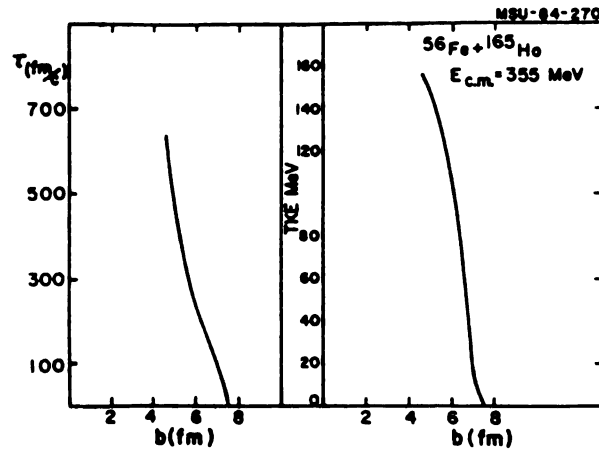


Fig.4. As fig.3 for the system $^{56}\text{Fe} + ^{165}\text{Ho}$.

attain thermal equilibrium. The above results suggest that the time required by the system to reach thermal equilibrium lies in the range 50 fm/c to 250 fm/c. Bertsch¹³⁾ has determined the time to reach local equilibrium, by considering the equilibration of a quadrupole deformation of the Fermi sphere within the Fermi-gas approximation. Our estimate is in good agreement with his numerical result.

4. Summary

In this contribution we have presented a simple classical model based on one-body dissipation. We assumed that during the reaction a neck is formed and we parametrized the radius of the neck by referring to the TDHF calculations.²⁻³⁾ An interesting feature of this model is the delayed-damping term. During the first stage, after neck formation, this implies that the motion is superfluid, while in the second stage a strong dissipation occurs arising from one-body dissipation (superviscosity).

Our model is in good agreement with experimental data on fusion cross-sections and the barrier to fusion at high Z^2/A is reproduced as well. Fast fission occurs in our model if a critical value of the interaction time is exceeded. Such a value is common to all systems.

Finally, the equilibration time for energy was estimated by referring to an experiment at 15 MeV/u .

We plan to extend the model by including fast-particle emissions in the early stage of the reaction and stochastic processes in deep inelastic scattering.

Acknowledgements

The author wishes to thank the RIFP-Kyoto for the warm hospitality and financial support.

References

- 1) G.F. Bertsch, MSU preprint (1982).
- 2) A. Bonasera, G.F. Bertsch and E.N. El Sayed, Phys. Lett. 141B (1984) 9.
- 3) A. Bonasera, submitted to Nucl. Phys. A.
- 4) A. Bonasera, submitted to Phys. Rev. Lett.
- 5) H. Stocker, private communication, and H. Stocker et al., Z. Phys. A306 (1982) 235.
- 6) T.C. Awes et al., Phys. Rev. Lett. 52B (1984) 251.
- 7) J. Randrup, Ann. Phys. (NY) 112 (1978) 356.
- 8) R. Bass, Phys. Rev. Lett. 39 (1977) 265.
- 9) W.J. Swiatecki, Nucl. Phys. A376 (1982) 275.
- 10) H. Doubre et al., Phys. Lett. 73B (1978) 135, and E. Tomas et al., Nucl. Phys. A373 (1982) 341.
- 11) R. Bock et al., Nucl. Phys. A388 (1982) 334.
- 12) K. Hildebrand, private communication and K. Hildebrand et al., Phys. Lett. 142B (1984) 212.
- 13) G.F. Bertsch, Z. Phys. A289 (1978) 103.

LIST OF REFERENCES

LIST OF REFERENCES

- [1] G.F. Bertsch, Les Houches, session XXX, 1977, pag. 177, vol I R. Balian & al. eds.
- [2] W. Norenberg, H.A. Weidenmuller, Introduction to the theory of Heavy-Ion Collisions, Springer Verlag.
- [3] R.A. Broglia, A. Winter, Heavy Ion Reactions, vol I. The Benjamin/Cummings Publishing Company.
- [4] M. Buhler & al., Workshop on Nuclear Dynamics III, Colorado 1984, pag. 105.
- [5] H. Ho & al., Submitted to Atoms and Nuclei.
- [6] P. Bonche & al., Phys. Rev. C20, 1979 (641)
- [7] W.J. Swiatecki, Nucl. Phys. A376, (1982) 275
- [8] S. Bjornholm & al., Nucl. Phys. A391, (1982) 471
- [9] M.B. Tsang & al., MSU preprint, Feb. 1983
- [10] Davies & al., Nuclear Physics with Heavy Ions, pag.57, 1983
- [11] A. Van Der Woude, Giant Multipole Resonances, vol. I pag. 65, Harwood Academic Publishers.
- [12] J.R. Nix & al., Phys. Rev. C21 (1980) 396
- [13] J.E. Poling & al., Phys. Rev. C13 (1979) 659
- [14] H. Stöcker & al., Z. Phys. A306 (1982) 235
- [15] A. Lazzarini & al., Phys. Rev. C24 (1981) 309
- [16] H. Doubre & al., Phys. Lett. 73B (1978) 135
- [17] E. Tomasi & al., Nucl. Phys. A373 (1982) 341
- [18] J. Barreto & al., Phys. Rev. C27 (1983) 1335
- [19] R. Bock & al., Nucl. Phys. A388 (1982) 334
- [20] M.B. Tsang & al., MSU preprint (1983)

- [21] J.R. Birkelund & al., Phys. Rev C27 (1983) 882
- [22] H.C. Britt & al., Phys. Rev. C13 (1976) 1483
- [23] H. Gauvin & al., Phys. Lett. 58B (1975) 163
- [24] B. Tamain & al., Nucl. Phys. A252 (1975) 187
- [25] C. Cabot & al., J. Physique 41 (1980), suppl. C10, 234
- [26] J.P. Bondorf & al., Nucl. Phys. A333 (1980) 285
- [27] A.K. Dhar & al., Nucl. Phys. A364 (1981) 105
- [28] A.K. Dhar & al., Phys. Rev. C25 (1982) 1432
- [29] T.C. Awes & al., Phys. Rev. Lett. 52B (1984) 251
- [30] G.F. Bertsch, Z. Phys. A289 (1978) 103
- [31] C.M. Ko & al., Phys. Lett. 77B (1978) 174
- [32] G. Münzerberg & al., Z. Phys. A300 (1981) 107